Received: 20 August 2019 | Accepted: 13 January 2020

DOI: 10.1002/jcp.29555

ORIGINAL RESEARCH ARTICLE

Journal of Cellular Physiology WILEY

Downregulation of uPAR promotes urokinase translocation into the nucleus and epithelial to mesenchymal transition in neuroblastoma

Ekaterina V. Semina[1,2] | Kseniya A. Rubina[1,3] | Anna A. Shmakova[1,2] | Karina D. Rysenkova[1,2] | Polina S. Klimovich[1,2] | Natalya A. Aleksanrushkina[1] | Veronika Y. Sysoeva[1] | Maxim N. Karagyaur[1] | Vsevolod A. Tkachuk[1,2]

[1]Department of Biochemistry and Molecular Medicine, Faculty of Medicine, Lomonosov Moscow State University, Moscow, Russia

[2]Laboratory of Molecular Endocrinology, Institute of Experimental Cardiology, Federal State Budgetary Organization National Cardiology Research Center Ministry of Health of the Russian Federation, Moscow, Russia

[3]Laboratory of Morohogenesis and Tissue Reparation, Faculty of Medicine, Lomonosov Moscow State University, Moscow, Russia

Correspondence
Kseniya A. Rubina, Lomonosov Moscow State University, Faculty of Medicine, Lomonosov av. 27/1, Moscow, Russia 119991.
Email: rkseniya@mail.ru

Funding information
Russian Foundation of Basic Research, Grant/Award Number: 17-04-00386; Russian Science Foundation, Grant/Award Number: 19-75-30007

Abstract

The urokinase system is involved in a variety of physiological processes, such as fibrinolysis, matrix remodeling, wound healing, and regeneration. Upon binding to its cognate receptor urokinase-type plasminogen activator receptor (uPAR), urokinase-type plasminogen activator (uPA) catalyzes the conversion of plasminogen to plasmin and the activation of matrix metalloproteases. Apart from this, uPA–uPAR interaction can lead to the activation of transcription factors, mitogen-activated protein kinase signaling pathways and RTK cascades. Elevated expression of uPA and uPAR is markedly associated with cancer progression and metastasis and correlates with a poor prognosis in clinics. Targeting the urokinase system has proved to be effective in experimental models in vitro and in vivo, however, in clinics the inhibition of the uPA/uPAR system has fallen short of expectations, suggesting that the question of the functional relevance of uPA/uPAR system is far from being moot. Recently, using CRISPR/Cas9 technology, we have shown that uPAR knockout decreases the proliferation of neuroblastoma Neuro2a cells in vitro. In the present study we demonstrate that uPAR expression is essential for maintaining the epithelial phenotype in Neuro2a cells and that uPAR silencing promotes epithelial-mesenchymal transition (EMT) and increased cell migration. Accordingly, uPAR knockout results in the downregulation of epithelial markers (E-cadherin, occludin, and claudin-5) and in the increase of mesenchymal markers (N-cadherin, α-smooth muscle actin, and interleukin-6). In search of the molecular mechanism underlying these changes, we identified uPA as a key component. Two key insights emerged as a result of this work: in the absence of uPAR, uPA is translocated into the nucleus where it is presumably involved in the activation of transcription factors (nuclear factor κB and Snail) resulting in EMT. In uPAR-expressing cells, uPAR functions as a uPA

"trap" that binds uPA on the cell surface and promotes controlled uPA internalization and degradation in lysosomes.

KEYWORDS

CRISPR/Cas9, epithelial–mesenchymal transition, neuroblastoma, urokinase, urokinase receptor

1 | INTRODUCTION

The plasminogen activator (PA) system comprises urokinase-type plasminogen activator (*PLAU* or uPA), its receptor (uPAR), plasminogen (the urokinase substrate), and the plasminogen activator inhibitors (PAI-1 and PAI-2; Choong & Nadesapillai, 2003; Fleetwood et al., 2014). Upon binding to uPAR, uPA is activated and catalyzes the conversion of plasminogen to plasmin (Ellis, Scully, & Kakkar, 1989). PA system is responsible for the degradation of the extracellular matrix, including basal membrane proteolysis, and in the activation of latent growth factors (Jaiswal, Varshney, & Yadava, 2018). uPA-dependent plasmin activation is blocked by PAI-1:uPAR:uPA:PAI-1 complex is rapidly internalized by LDL receptor-related protein 1 (LRP-1) and is followed by uPA and PAI-1 degradation in lysosomes (Cortese, Sahores, Madsen, Tacchetti, & Blasi, 2008; Czekay, Kuemmel, Orlando, & Farquhar, 2001). The PA system participates in a variety of physiological processes, such as clot lysis (Chapin & Hajjar, 2015), wound healing (Montuori & Ragno, 2009), embryo development (Teesalu, Blasi, & Talarico, 1996), and tissue remodeling and regeneration (Blasi & Sidenius, 2010; Solberg, Ploug, Høyer, Hansen, Nielsen, & Lund, 2001). At the same time, uPA and uPAR are involved in the pathogenesis of various diseases (Jaiswal et al., 2018; Manetti et al., 2014; Mekkawy, Pourgholami, & Morris, 2014; Santibanez, 2013).

uPA/uPAR system is recognized to be a powerful driver of cancer progression (Jaiswal et al., 2018; Ulisse, Baldini, Sorrenti, & D'Armiento, 2009). uPAR polarizes uPA proteolytic activity to the leading edge, thus facilitating cancer cell migration and invasion (Jaiswal et al., 2018; Mekkawy et al., 2014). Apart from this, uPA–uPAR interaction can lead to activation of the Ras-Raf-MEK-ERK signaling pathway, which is involved in altered cancer cell adhesion and migration, and in enhanced proliferation and metastasis (Luo et al., 2011). Although the underlying mechanisms are far from being fully elucidated, uPAR was shown to be involved in epithelial–mesenchymal transition (EMT) in breast cancer cells. Using human breast cancer MDA-MB-468 cell line that has an epithelial phenotype, uPAR was demonstrated to promote EMT under hypoxic conditions through the activation of signal transduction involving extracellular signal-regulated kinase 1/2 (ERK1/2) and phosphoinositide 3-kinase (PI3K; Chandrasekar et al., 2003; Nguyen, Hussaini, & Gonias, 1998). In contrast, in MDA-MB-231 breast cancer cells that express the high level of uPAR and exhibit mesenchymal phenotype, the sustained uPAR expression is required, since uPAR knockdown results in the reversal of the phenotype to epithelial (Jo et al., 2009). Interestingly, the uPA/uPAR system contributes to the EMT program independently from uPA enzymatic activity, particularly through activation of uPAR-induced intracellular signaling (Montuori et al., 2016).

uPAR is considered to be a key component of the signalosome, which comprises such molecules as Src, Akt, FAK (focal adhesion kinase), and others (Degryse, 2008). uPAR can also interact laterally with different receptor tyrosine kinases, such as platelet-derived growth factor receptor and epithelial growth factor receptor, G-protein coupled receptor, vitronectin, and integrins (αvβ3, αvβ, α5β1, and α3β1) affecting intracellular signaling, proliferation, cell adhesion, and migration (Jaiswal et al., 2018; Montuori et al., 2016).

uPA and uPAR expression are demonstrably increased in a variety of malignant tumors and a positive correlation between its increased level and poor prognosis has been reported (Mekkawy et al., 2014; Montuori et al., 2016; Sliva, 2004). Despite the abundance of experimental research aimed at inhibiting the uPA/uPAR system, including research on selective uPA inhibitors, microRNAs, antagonist peptides, monoclonal antibodies able to disrupt uPA–uPAR binding, gene therapy techniques, and CRISPR/Cas9 technology silencing expression of uPA or uPAR (Gondi et al., 2004; Mekkawy et al., 2014; Montuori et al., 2016; Rabbani et al., 2010; Rysenkova et al., 2018; Ulisse et al., 2009), the targeting of the urokinase system in clinics has fallen short of expectations. Furthermore, some experimental data has emerged indicating that suppression of the urokinase system activity can augment tumor growth (Sugiura et al., 1999). Therefore, unraveling other potential molecular mechanisms involved in the regulation of urokinase system activity and their role in EMT may result in a refined understanding of cancer biology and improved outcomes in cancer treatment.

In this study, we demonstrate that uPAR silencing in murine neuroblastoma Neuro2a cells promotes the EMT program, including diminished expression of epithelial markers (E-cadherin, occludin, and claudin-5) and upregulated expression of mesenchymal markers (EMT-transcription factors nuclear factor κB [NF-κB] and Snail, N-cadherin and α-smooth muscle actin [α-SMA]). uPAR deficiency results in the alteration of cell morphology and signal transduction, and enhanced migration but reduced colony-forming potential. In search of the molecular mechanism responsible for these changes, we identified uPA as a central component and a new regulator. We hypothesize that uPAR functions as a uPA "trap" that promotes uPA internalization and degradation in lysosomes, while in the absence of uPAR, uPA are translocated into the nucleus where it can be involved in the regulation of gene expression. The complicated signaling regulatory network revealed in the present study indicates the existence of a functional link between the urokinase system and the EMT program. Further studies are needed to clarify the exact mechanisms of activated signal transduction mediated by the urokinase system, which may help to assign molecular signatures of neuroblastoma.

2 | EXPERIMENTAL PROCEDURES

2.1 | Neuro2a cell culture

Mouse Neuro2a neuroblastoma cells (CCL-131™, RRID: CVCL_0470; ATCC) were maintained in complete medium: Dulbecco's modified Eagle's medium (Hyclone) supplemented with 10% fetal bovine serum, 1X minimum essential medium non-essential amino acids solution, and 1X antibiotic–antimycotic solution (all from Gibco). Cells were plated at a concentration of 1×10^5 cells/ml. Cells were enrolled in the experiments before the 20th passage.

2.2 | CRISPR/Cas9 uPAR gene (*PLAUR*) downregulation in Neuro2a cells

Neuro2a cell clones with downregulated uPAR or complete uPAR knockout were obtained as described earlier (Rysenkova et al., 2018). To obtain uPAR-deficient clones, single-cell dilution of transfected cells and clone expansion were performed. For further experiments, three clones out of 30 were selected: Neuro2a-ΔuPAR clone #6 with complete uPAR knockout and clones #3 and #30 with significant uPAR suppression (Rysenkova et al., 2018).

2.3 | uPAR overexpression and downregulation in Neuro2a cells using plasmid vectors

The detailed procedure of overexpression and downregulation of uPAR in Neuro2a cells was published by us previously (Semina et al., 2016). Briefly, to suppress endogenous uPAR expression we used a commercially-available plasmid vector encoding shRNA (uPAR shRNA Plasmid [m], cat# sc-36782-SH; Santa Cruz). For uPAR overexpression, a pN1 vector encoding full-length murine uPAR DNA (pN1-uPAR) was used. Cell transfection was performed following the Lipofectamine 2000 (Life Technologies) protocol. After transfection, cells were cultured for 8 weeks in a complete medium containing selective antibiotics: Puromycin for Neuro2a-shuPAR (at 4 μg/ml; Sigma-Aldrich) and G418 for Neuro2a-uPAR cells (at 400 μg/ml; Sigma-Aldrich). uPAR expression was assessed using real-time polymerase chain reaction (RT-PCR).

2.4 | uPAR re-expression after CRISPR/Cas9 *PLAUR* gene downregulation in Neuro2a cells

For uPAR re-expression in uPAR-deficient clones (Neuro2a-ΔuPAR clones #3, #6, and #30), we used pN1 vector encoding full-length murine uPAR complementary DNA (cDNA) as previously described (Semina et al., 2016). Briefly, cell transfection was performed using Lipofectamine 2000 (Life Technologies). After re-expression, uPAR clone cells (Re#3, Re#6, Re#30) were cultured for 8 weeks in complete medium containing G418 (400 μg/ml; Sigma-Aldrich) as a selective antibiotic. uPAR expression was evaluated by RT-PCR.

2.5 | Cell lysates and western blot analysis

Cells were lysed in a Laemmli buffer containing β-mercaptoethanol, heated at 90°C for 10 min, electrophoresed in 10% sodium dodecyl sulfate/polyacrylamide gel and electroblotted onto polyvinylidene difluoride membranes (Immobilon). Kaleidoscope Prestained Standards (Bio-Rad) were used as molecular weight markers. After rinsing in Tris-buffer saline (TBS), membranes were pre-blocked in an incubation TBSM buffer (TBS containing 5% nonfat dry milk and 0.5% Tween-20) for 2 hr. Membranes were incubated with the following antibodies: rabbit anti-uPAR (cat# SC-10815, RRID:AB_2165354; Santa Cruz), mouse anti-occludin (cat# 33–1500, RRID:AB_2533101; Invitrogen), mouse anti-claudin-5 (cat# 35-2500, RRID:AB_2533200; Invitrogen), rabbit anti-E-cadherin (cat# Ab53033, RRID:AB_868611; Abcam), rabbit anti-vinculin (cat# V4139, RRID:AB_262053; Sigma-Aldrich), rabbit anti-N-cadherin (cat# Ab76011, RRID:AB_1310479; Abcam), rabbit anti-interleukin-6 (anti-IL-6; cat# ab7737, RRID:AB_306031; Abcam), rabbit anti-α-SMA (cat# Ab32575, RRID:AB_722538; Abcam), rabbit anti-total ERK1/2 (cat# ab17942, RRID:AB_2297336; Abcam), rabbit anti-phospho-ERK (anti-p-ERK; T185+T202; cat# ab4819, RRID:AB_304655; Abcam), rabbit anti-signal transducer and activator of transcription 1 (anti-STAT1; cat# 9172, RRID:AB_2198300; Cell Signaling), rabbit anti-p-SMAD2 (cat# ab53100, RRID:AB_874025; Abcam), rabbit anti-p-SMAD3 (cat# ab52903, RRID:AB_882596; Abcam), rabbit anti-NF-κB p105/p50 (cat# ab7971, RRID:AB_306185; Abcam) and rabbit histone H3A (cat# ab18521, RRID:AB_732917; Abcam) at 4°C for 24 hr, washed with TBSM, and incubated with secondary antibodies conjugated with peroxidase (Imtek) at room temperature for 1 hr. Membranes were visualized using SuperSignal West Pico Chemiluminescent Substrate (Thermo Fisher Scientific) and ChemiDoc™ XRS+ System (Bio-Rad) for western blot analysis imaging and analysis.

2.6 | Subcellular fractionation

Cellular fractions (membrane, cytosolic, and nuclear) obtained from Neuro2a cells were extracted using the Qproteome™ Cell Compartment kit according to the manufacturer's instructions (Qiagen). Protein concentration in each fraction was measured using the BCA protein assay kit (Pierce Biotechnology). Lysates were subjected to western blot analysis.

2.7 | Quantitative real-time polymerase chain reaction analysis

RNeasy® Mini Kit (Qiagen) was used for total RNA extraction. For cDNA preparation, 1,5 μg of total RNA was used. The cDNA synthesis was carried out using SuperScript® III First-Strand Synthesis SuperMix for quantitative RT-PCR (qRT-PCR; Thermo Fisher Scientific) MMLV RT kit (Evrogen, Russia). The concentration of undiluted cDNA in qPCR reaction volume was 8%. Primers for murine uPAR, Snai1, and self-renewal regulatory factors Nanog, Oct4, Sox2, and β-actin (used as an endogenous

control gene) cDNAs were obtained from Evrogen: uPAR-Forward 5′-CGCCACAAACCTCTGCAAC-3′, uPAR-Reverse 5′-CTCTGTAGGATAGCGGCATTG-3′, uPA-Forward 5′-ATGGAAATGGTGACTCTTACCGA-3′, uPA-Reverse 5′-TGGGCATTGTAGGGTTTCTGA-3′, Snai1-Forward 5′-CTGCTTCGAGCCATAGAACTAAAG-3′, Snai1-Reverse 5′-GAGGGGAACTATTGCATAGTCTGT-3′ (Li et al., 2011), Oct4-Forward 5′-TTGGGCTAGAGAAGGATGTGGTT-3′, Oct4-Reversed 5′-GGAAAAGGGACTGAGTAGAGTGTGG-3′, Nanog-Forward 5′-CAAAGGATGAAGTGCAAGCG-3′, Nanog-Reversed 5′-CCAGATGCGTTCACCAGATAG-3′, Sox2-Forward 5′-GCGGAGTGGAAACTTTTGTCC-3′, Sox2-Reversed 5′-CGGGAAGCGTGTACTTATCCTT-3′, Snail, β-actin-Forward 5′-AGTGTGACGTTGACATCCGTA-3′, β-actin-Reverse 5′-GCCAGAGCAGTAATCTCCTTCT-3′. The thermal cycling program for template denaturation, primers annealing and primer extension was 94°C for 15 s, 62°C for 15 s, and 72°C for 20 s for 40 cycles, correspondingly. A relative transcript level was calculated using the $2^{-\Delta\Delta C_t}$ method. The normalization was done assuming the mean level of each transcript in wild-type (WT) cells to be 1.

2.8 | Cell index measurement with automated incucyte® ZOOM analysis system

Incucyte® ZOOM Live Cell Analysis System (Essen Bioscience) is an automated cell culture monitoring system (microscope + imaging controller) located inside a CO_2 incubator. The method allows measuring the changes in the cell confluence index in real-time, reflecting the changes in cells' number or their size. Neuro2a cells were plated in 12-well plates (concentration of cells 3×10^5/well) and placed in the Incucyte® ZOOM system. The time-lapse imaging of nine fields of vision in each well was carried out for 5 days with a frequency of every 2 hr. The curves reflecting the changes in the monolayer area over time were obtained using the Incucyte® ZOOM image-processing software package. Briefly, the Incucyte ZOOM's Confluence Processing Analysis tool is based on area (confluence) metrics and allows calculating the value of the area covered by cells (mean percentage of cell area in each well).

2.9 | Neuro2a cells proliferation assay

Neuro2a cells were plated in 24-well plates (concentration of cells 2×10^4/well) and maintained in the complete medium. The number of cells in cultures with different uPAR expression was calculated every 24 hr for 4 days using an automatic Countess® Automated Cell Counter (Thermo Fisher Scientific). The proliferation of histogram was plotted using the obtained data. Data are presented as the dependence of total cell number on the time interval. The experiment was performed in six parallels and repeated three times.

2.10 | Neuro2a cell size measurement

Neuro2a cells with different uPAR expression were plated into 24-well plates at a concentration of 1×10^4/well. After 48 hr, cells were moved into the chamber of a Leica microscope (Leica AF6000 LX) equipped with a temperature (37°C) and CO_2 (5%) control system, camera Leica DFC 350FX and LAS AF software. Images of living cells were captured using a Leica phase-contrast light microscope (Leica AF6000 LX). The cell size (cell area) was evaluated using the ImageJ software (RRID: SCR_003070; National Institute of Health, Bethesda, MD). Minimal cell size was limited to 50 μm^2 to avoid false-positive measuring of small dots in the image; cells on the image edges were excluded. Inaccurately selected cells that appeared as a result of the automated method of ImageJ application (Baviskar, 2011) were excluded and re-selected manually using the Selection Brush Tool (ImageJ tool). The areas of at least 200 cells were measured for each cell type.

2.11 | Cell adhesion assay

Neuro2a cells with different levels of uPAR expression were plated into 24-well plates at a concentration of 2×10^5/well. Cells were incubated in complete medium for 30 min, 1 or 2 hr at 37°C. Unattached cells were removed by a brief rinse with Hank's balanced saline solution (HBSS) and a change of the medium. Images of attached cells in 3–5 equivalent fields of view for each well were captured using a time-lapse Leica phase-contrast light microscope (Leica AF6000 LX) equipped with a stage incubator with temperature (37°C) and CO_2 (5%) control, Leica DFC 350FX camera, and LAS AF software. The number of attached cells for each image was calculated using the ImageJ software. The experiment was performed in three biological replicates.

2.12 | Wound scratch assay

Neuro2a cells with different levels of uPAR expression were plated into 24-well plates at a concentration of 1×10^4/well and allowed to reach a confluent monolayer up to 48 hr. To create a "scratch," the cell monolayers were scraped in a straight line with a p1000 pipet tip. Immediately afterward, the media was replaced with a fresh growth media containing either 50 nM uPA, bovine serum albumin (BSA) in equivalent concentration as control or 10 μM highly specific uPA inhibitor BC11 (IC50 8.2 μM). Cells were analyzed using a time-lapse Leica phase-contrast light microscope (Leica AF6000 LX) equipped with a stage incubator with temperature (37°C) and CO_2 (5%) control, Leica DFC 350FX camera, and LAS AF software. Images of living cells were acquired every 10 min during the next 24 hr. For each cell type, the wound area was measured using the ImageJ software and the magnetic resonance imaging wound healing tool (http://dev.mri.cnrs.fr/projects/imagej-macros/wiki/Wound_Healing_Tool) at the beginning of the experiment (0 hr) and 24 hr after. The data were expressed as the change in the wound area over time and calculated as a percentage of the original wound area. Experiments were performed in duplicates and repeated twice.

2.13 | Immunofluorescent staining and confocal imaging of Neuro2a cells

Neuro2a cells with different levels of uPAR expression were seeded into the wells of the Nunc® Lab-Tek® Chamber Slide™ system at a low concentration (2×10^4/ml) in a complete medium; 24 hr later the slides with cells were washed with warmed HBSS, fixed in 4% formaldehyde, and incubated with primary and secondary antibodies. Co-staining of Neuro2a cells for intracellular uPA (mouse monoclonal anti-uPA; Abcam) and lysosome-associated membrane marker (rabbit anti-LAMP1; Abcam), was performed in permeabilizing conditions using Triton X-100 (0.1% in HBSS, 10 min) as described earlier (Semina et al., 2016). Donkey anti-rabbit AlexaFluor® 488 and donkey anti-mouse AlexaFluor® 594 (Molecular Probes) were used as secondary antibodies. The nuclei were counterstained with DAPI (Sigma-Aldrich). Images were acquired using a confocal laser scanning microscopy system (LSM 780; Zeiss) and ZEN 2010 software. All images were captured with the same confocal gain and offset settings. The fluorescence intensity data were processed using Histo function of ZEN 2010 software. The Histo function allows the acquisition of the distribution of pixel intensities along the marked line or in the region of interest of the image. The Histo function displays statistical parameters of pixel intensities, such as mean intensity, standard deviation, number of pixels, and size area. The results of at least three independent experiments are presented.

To address the possibility of exogenous uPA to be translocated into nuclei, Neuro2a cells with different levels of uPAR expression were seeded into the wells of the Nunc® Lab-Tek® Chamber Slide™ system at a concentration of 2×10^4/ml in a complete medium. After 24 hr 50 nM of urokinase conjugated with fluorescein (uPA-fluorescein isothiocyanate [FITC]) was added to the wells. After 30 min, 6 hr, and 24 hr the cells were washed with warmed HBSS, fixed in 4% formaldehyde and incubated with primary anti-LAMP1 (rabbit; Abcam) and secondary AlexaFluor® 594 antibodies (donkey anti-rabbit). The nuclei were counterstained with 4′,6-diamidino-2-phenylindole (DAPI). Images were acquired using a confocal laser scanning microscopy system (LSM 780; Zeiss) and ZEN 2010 software. All images were captured with the same confocal gain and offset settings.

2.14 | Neuro2a colony-forming assay

To evaluate the colony-forming potential, a single-cell suspension of Neuro2a cells with different uPAR expression was plated on 24-well plates in complete cell medium at a density of 1×10^4/well. Cells of each type were plated in at least two wells and repeated three times. After 48 hr, the number of colonies (CFU) was analyzed in at least five fields of view of each cell type. Imaging was carried out using a Leica phase-contrast light microscope (Leica AF6000 LX).

2.15 | Data and statistical analysis

All quantitative data are presented as the mean ± standard error of the mean (*SEM*) or standard deviation. Student's unpaired *t* test was applied for two-group comparisons. For multiple-group comparisons we performed one-way analysis of variance (ANOVA) if the hypothesis of the equal variances was accepted; Welch's ANOVA was used if the hypothesis of the equal variances was rejected, followed by the Tukey or Tamhane's T2 post hoc tests, respectively, to determine the statistical significance of the obtained results. A two-way ANOVA followed by the Tukey post hoc test was performed for cell adhesion analysis and wound scratch assay. Data were analyzed using GraphPad

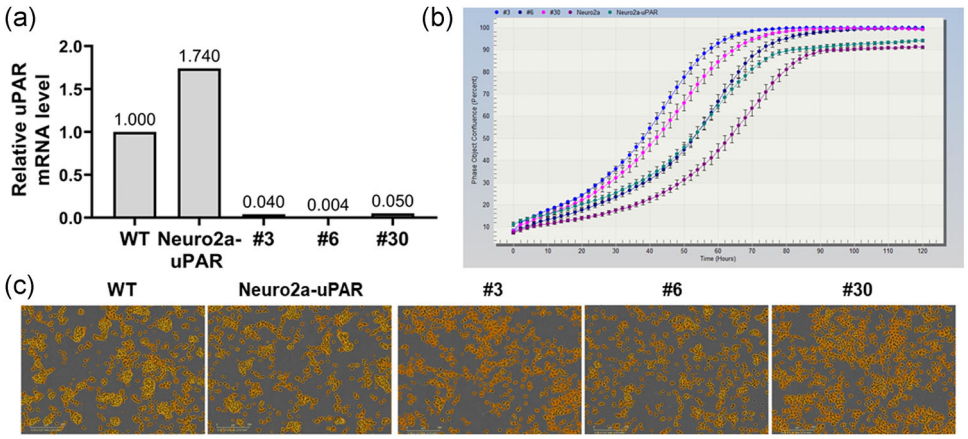

FIGURE 1 The area covered by cells evaluated by the IncuCyte ZOOM™ system in Neuro2a cell cultures with different levels of uPAR expression. (a) RT-PCR analysis of uPAR expression in Neuro2a cells. The mRNA level in Neuro2a was evaluated using RT-PCR; data were normalized to β-actin expression as a housekeeping gene. Results are representative of three independent experiments. (b) The time-lapse imaging was performed continuously during 120 hr. The curves reflect the changes in the monolayer area over time. Data are presented as mean ± *SEM*. (c) Automatically identified regions of interest using masks (yellow) after 24 hr. Bars, 300 μm. WT: control Neuro2a cells; Neuro2a-uPAR: uPAR-overexpressing Neuro2a cells; #3, #6, and #30: uPAR-deficient clones of Neuro2a cells. RT-PCR, real-time polymerase chain reaction; *SEM*, standard error of mean; uPAR, urokinase-type plasminogen activator receptor; WT, wild-type

Prism 8 software (RRID: SCR_002798; GraphPad Software Inc.). A value of $p < .05$ was considered to be statistically significant.

3 | RESULTS

3.1 | Neuro2a cells' morphology depends on uPAR expression

We used IncuCyte™ for live monitoring of Neuro2a cells with different levels of uPAR expression.

As described earlier, we generated Neuro2a-uPAR cells stably overexpressing murine uPAR using plasmid transfection (Semina et al., 2016). Recently, we also reported the generation of uPAR-deficient Neuro2a cell clones using the CRISPR/Cas9 gene-editing technique (Neuro2a-ΔuPAR cells; Rysenkova et al., 2018). In the present study, we used three of these clones: #6 with complete uPAR knockout, and clones #30 and #3 with significant uPAR suppression (in #3 clone uPAR mRNA was 25 times less than in WT, while in #30 clone it was 20 times less) (Figure 1a). To support the data obtained using uPAR-deficient clones generated with CRISPR/Cas9 technology, we also enrolled Neuro2a cells (Neuro2a-shuPAR)

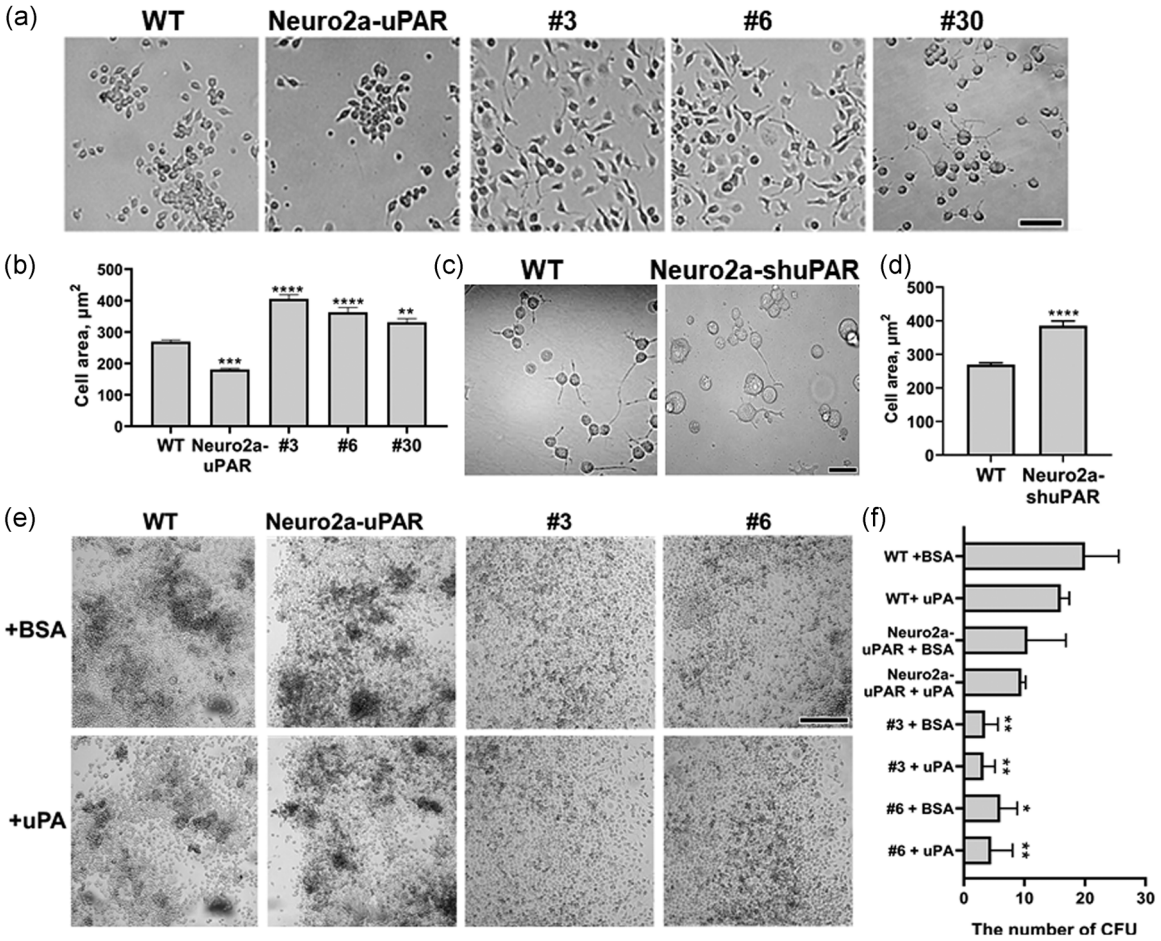

FIGURE 2 Expression of uPAR affects cell morphology in Neuro2a cells. (a) Neuro2a cells with different levels of uPAR expression were plated in 24-well plates at a concentration of 1×10^4/well. 48 hr after the cells were monitored using a light microscope. Results are representative of three independent experiments. Bar 75 μm. (b) Results of cell size (cell area) measurement; minimal cell size was limited to 50 μm^2 to avoid measuring too small dots. (c) Control Neuro2a cells (WT) and cells transfected with shRNA to suppress uPAR (Neuro2a-shuPAR) were plated onto 24-well plates at a concentration of 0.5×10^4/well. 48 hr later, cells have been monitored using light microscopy. The silencing of uPAR in Neuro2a cells leads to the emergence of atypical cells of large size. Results are representative of three independent experiments. Bar 50 μm. (d) Results of cell size (cell area) measurement; minimal cell size was limited to 50 μm^2 to avoid measuring unrelated dots. (e) Neuro2a cells with different uPAR expression were seeded into cell culture plates in the presence of 50 nM uPA or BSA as a control. 24 hr later, cells were analyzed using light microscopy. Bar 250 μm. Results are representative of three independent experiments. (f) Graph showing the number of colony-forming units (CFU) calculated at least in three fields of view. The cell colony-forming ability of Neuro2a depends on the uPAR expression. Data are presented as mean ± *SEM*, $^*p < .05$ compared with WT, $^{**}p < .01$ compared with WT, $^{***}p < .001$ compared with WT, $^{****}p < .0001$ compared with WT (ANOVA, Tukey post hoc test). WT: control Neuro2a cells; Neuro2a-uPAR: uPAR-overexpressing Neuro2a cells; #3, #6, and #30: uPAR-deficient clones of Neuro2a cells. ANOVA, analysis of variance; BSA, bovine serum albumin; *SEM*, standard error of mean; shRNA, short hairpin RNA; uPA, urokinase-type plasminogen activator; uPAR, urokinase-type plasminogen activator receptor; WT, wild-type;

with downregulated uPAR expression that had been acquired using the shRNA technique as described earlier (Semina et al., 2016).

An image-based method for real-time monitoring of cell index using IncuCyte™ and ImageJ analysis allowed us to demonstrate that uPAR is a major trigger of the changes in Neuro2a cell morphology. Cells were plated as described in Section 2 and allowed to adhere. IncuCyte™ analysis assigned an increased cellular index to uPAR-deficient cells (#3, #6, and #30 clones in Figure 1b) throughout the experiment (120 hr). Interestingly, uPAR-overexpressing cells were also characterized by an increased cell index (120 hr). Since the evaluation of the cell index by the IncuCyte™ system is based on the mask used to characterize the surface area occupied by cells (Figure 1c), the augmentation in cell index can reflect the increased cell number and/or the enlargement in their size.

To address this matter, Neuro2a cells with different uPAR expression levels were plated in a low-density monolayer and cultured for 24 hr allowing strong cell adhesion. Images of living cells were captured using a Leica microscope (Figure 2a) and the cell size was analyzed with the tools of ImageJ (Figure 2b). We found that the size of Neuro2a-ΔuPAR cells (#3, #6, and #30 clones) was significantly larger in respect to the size of WT cells, while the size of Neuro2a-uPAR cells was, on the contrary, significantly smaller (Figure 2b). After 24 hr in culture, cell area in uPAR-deficient clones #3, #6, and #30 was 406,0 ± 12,9 μm^2 ($p < .0001$ compared with WT cells; ANOVA), 362,9 ± 15,3 μm^2 ($p < .0001$ compared with WT cells; ANOVA), and 331,2 ± 11,4 μm^2 ($p < .01$ compared with WT cells; ANOVA), respectively; while in WT cells, cell area was 269,5 ± 5,6 μm^2 and in Neuro2a-uPAR cells, the cell area was 181,2 ± 3,4 μm^2 ($p < 0.001$ compared with WT cells; ANOVA).

To avoid the effects related to the individual features of the selected clones #3, #6, and #30, we repeated the experiment using Neuro2a cells, where uPAR expression had been silenced by RNA interference. As anticipated, the cell size of Neuro2a-shuPAR cells was significantly larger compared to WT cells (Figure 2c). After 24 hr in culture, the cell size of Neuro2a-shuPAR cells was 384,9 ± 14,5 μm^2 ($p < .0001$ compared with WT cells; ANOVA), while in WT cells the cell area was 269,5 ± 5,6 μm^2 (Figure 2d). Thus one can infer that uPAR expression demonstrably alters Neuro2a cell morphology: uPAR downregulation using the CRISPR/Cas9 gene-editing technique and RNA interference results in a significant enlargement in the cell size, while uPAR overexpression leads to the opposite effect—a reduction in the cell size.

3.2 | uPAR regulates cell proliferation in Neuro2a cells

As described above, the cell size of uPAR-overexpressing cells (Neuro2a-uPAR) was significantly diminished comparing to the control (WT; Figure 2). We anticipated that the reduction in the cell size could be accompanied by an increase in cell proliferation in uPAR-overexpressing cells. To prove this assumption, Neuro2a-uPAR and WT cells were plated in equal concentration and analyzed using an automatic Countess® Automated Cell Counter (Thermo Fisher Scientific). The rise in cell proliferation was evident from the data of total cell counts at different time points (24–96 hr; Figure 3). After

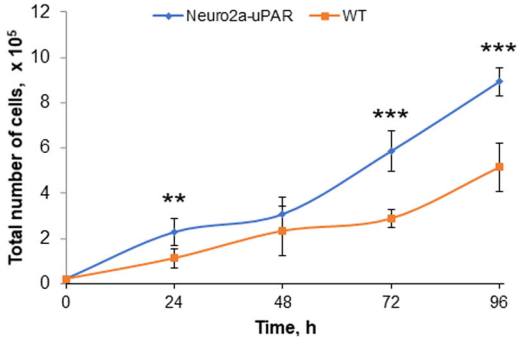

FIGURE 3 uPAR overexpression increases the proliferation of Neuro2a cells. WT—Control Neuro2a cells; Neuro2a-uPAR—uPAR-overexpressing cells. The data are presented as mean ± *SD* ($n = 6$ wells per group). **$p < .01$ compared with WT, ***$p < .001$ compared with WT (*t* test). *SD*, standard deviation; uPAR, urokinase-type plasminogen activator receptor; WT, wild-type

96 hr up to 1.73 times difference in the cell numbers was evident between WT and Neuro2a-uPAR cells ($p < .001$ compared with WT, *t* test).

We have shown previously that uPAR deficiency correlates with the decline in cell proliferation as measured by live cell counts and Flow Cytometry analysis using an antibody against Ki-67 at different time points (Rysenkova et al., 2018). To summarize, our data obtained previously and in the current study indicate that uPAR suppression results in the increased cell index, which is due to the enlargement in the cell size and the decrease in cell proliferation.

It is common knowledge that the change in cell phenotype and increased proliferation frequently correlate with EMT in cancer cells (Hanahan & Weinberg, 2011). To gain further understanding of the role of uPAR in EMT of neuroblastoma cells, we evaluated cell migration capacity in wound scratch assay, colony-forming potential, the expression level of transcription factors responsible for plur-ipotency and self-renewal, expression of EMT markers, and signaling activated upon EMT in relation to the level of uPAR expression.

3.3 | uPAR suppression significantly reduces colony-forming potential in Neuro2a cells

The CFU assay is the most frequently used test to assess the clonogenic potential of bone marrow and tumor cells (Kurtzberg et al., 2008). To compare the clonogenic potential of uPAR-expressing cells (WT and uPAR-overexpressing Neuro2a-uPAR cells) with uPAR-deficient cells (clones #3 and #6 of Neuro2a-ΔuPAR), we plated them in a low-density monolayer and treated with BSA for 24 hr (control) or uPA at 50 nM (Figure 2E). CFU was 20 ± 3 in WT cells treated with BSA (WT + BSA) and 16 ± 1 in WT cells treated with uPA (WT + uPA); in uPAR-overexpressing cells, CFU was 11 ± 5 in cells treated with BSA (Neuro2a-uPAR + BSA) and 10 ± 0.5 in cells treated with uPA (Neuro2a-uPAR + uPA); in uPAR-deficient clones, CFU was 4 ± 2 in clone #3 treated with BSA (#3 + BSA) and 3 ± 1 in clone #3 treated with uPA (#3 + uPA), 6 ± 2 in clone #6 treated with BSA (#6 + BSA) and 5 ± 3

in clone #6 treated with uPA (#6 + uPA; Figure 2f). The mean total CFU in clones #3 and #6, either treated with BSA or uPA, was significantly lower comparing to WT cells ($p < .05$; ANOVA). Remarkably, the administration of uPA exerted no statistically significant effect on the number of CFU formed by control cells, uPAR-deficient or uPAR-overexpressing cells ($p > 0.05$; ANOVA). Overall, these results indicate that uPAR expression is crucial for the colony-forming potential of Neuro2a cells, since uPAR-deficient clones exhibit a markedly reduced CFU.

3.4 | Quantitative RT-PCR of *Nanog*, *Oct4*, and *Sox2* in Neuro2a cells

Quantitative RT-PCR was conducted to determine the relative expression levels of three transcription factors *Nanog*, *Oct4*, and *Sox2*, since their expression correlates with cell clonogenic potential and stem cell-like phenotype (Carlin, Davis, Weiss, Schultz, & Troyer, 2006; Gagliardi et al., 2013; Osorno & Chambers, 2011; Walker & Stanford, 2009). Results from one experiment are presented as mean ± *SEM* (Table 1). The results indicate that there was no statistically significant difference in *Nanog* mRNA expression levels between the cell types (control cells, uPAR-overexpressing cells, and uPAR-deficient clones, #3, #6, and #30 clones; $p > .05$; ANOVA). Furthermore, mRNA for *Oct4* and *Sox2* was undetectable in all the tested cell types. Thus, we can infer from these data that, while uPAR downregulation resulted in the decreased colony-forming potency of Neuro2a cells, it had no effect on the mRNA expression levels of transcription factors responsible for pluripotency and self-renewal (*Nanog*, *Oct4*, and *Sox2*). Thus, the increase in the proliferation rate of uPAR-overexpressing cells is not interrelated with the change in the expression of transcription factors responsible for pluripotency but is rather associated with the colony-forming ability.

TABLE 1 RT-PCR analysis of expression of stem cell pluripotency markers in Neuro2a cells; RT-PCR data are presented as fold-change in *Nanog*, *Oct4*, and *Sox2* relative gene expression.

	Relative mRNA level		
Cell type	***Nanog***	***Oct4***	***Sox2***
WT	1.000 ± 0.132	Not detectable	Not detectable
Neuro2a-uPAR	1.251 ± 0.453	Not detectable	Not detectable
#3	0.316 ± 0.262	Not detectable	Not detectable
#6	0.972 ± 0.099	Not detectable	Not detectable
#30	0.178 ± 0.061	Not detectable	Not detectable

Note: Data were normalized to β-actin expression as a housekeeping gene; the normalization was done assuming as 1 the mean level of transcript in WT cells. Data are presented as a mean ± *SEM*. WT: control Neuro2a cells; Neuro2a-uPAR: uPAR-overexpressing cells; #3, #6, and #30: uPAR-deficient clones of Neuro2a cells.

Abbreviations: mRNA, messenger RNA; RT-PCR, real-time polymerase chain reaction; *SEM*, standard error of mean; uPAR, urokinase-type plasminogen activator receptor; WT, wild-type.

3.5 | uPAR expression affects Neuro2a cell adhesion

Neuro2a cells with different levels of uPAR expression were seeded at equal concentrations into 24-well plates; non-adherent cells were discarded after 30 min, 1 hr, or 2 hr by HBSS rinsing and media replacement (Figure 4a). After 30 min both, WT and Neuro2a-uPAR cells were well attached: 837 ± 153 and 1316 ± 123 cells per image view, respectively. However, fewer cells attached in uPAR-deficient cultures: 732 ± 130 in Neuro2a-shuPAR cells, 647 ± 110 in clone #3, 431 ± 92 in clone #6, and 151 ± 30 in clone #30 (Figure 4b). The differences between WT and clone #30 were statistically significant ($p < .05$; two-way ANOVA). The differences between uPAR-overexpressing cells (Neuro2a-uPAR) and all uPAR-deficient cells (Neuro2a-shuPAR, clones #3, #6, #30) were statistically significant ($p < .05$, $p < .01$, $p < .0001$, $p < .0001$, correspondingly; two-way ANOVA).

After 1 hr incubation, Neuro2a-uPAR cells (14667 ± 272 per image view) adhered significantly stronger than WT cells (753 ± 173; $p < .05$; two-way ANOVA). The number of cells attached to plastic in Neuro2a-uPAR cell culture was statistically higher than in Neuro2a-shuPAR culture (623 ± 104) or clone #3 (495 ± 83) or clone #6 (668 ± 132) or clone #30 (241 ± 61) ($p < .001$, $p < .0001$, $p < .001$, $p < .0001$, correspondingly; two-way ANOVA). However, after 2 hr no differences in cell adhesion between different cell types can be detected, reflecting that 2 hr time interval was enough for Neuro2a cells to attach ($p > .05$; two-way ANOVA). Furthermore, when we compared the differences between cell adhesion after 30 min, one or 2 hours, we found that cell adhesion changed significantly between time points only in clones #3, #6, and #30 ($p < .05$; two-way ANOVA), which was consistent with our microscopic live observation that uPAR-deficient cells had a lower adhesion capacity and needed more time to fully attach to a culture plate. One the contrary, uPAR overexpression resulted in an increase in cell adhesion.

3.6 | uPAR downregulation increases Neuro2a cell migration in wound scratch assay

We further examined the migration potential of Neuro2a cells with different uPAR expression levels using a standard in vitro wound scratch assay (Liang, Park, & Guan, 2007). Green areas in Figure 4c indicate the wound surfaces at the beginning of the experiment (0 hr) and 24 hr later. As illustrated in Figure 4c, uPAR-expressing cells (WT and Neuro2a-uPAR) generally displayed a low migratory ability in control conditions (BSA); no statistically significant difference in migration rate was detected between these cells at 24 hr ($p > .05$; two-way ANOVA; Figure 4d). uPA exerted no stimulatory effects on wound healing in uPAR-expressing cell cultures: administration of 50 nM urokinase failed to increase the migratory rate of WT or Neuro2a-uPAR cells ($p > .05$; two-way ANOVA). Strikingly, in control conditions (BSA) the cell migration capacity of Neuro2a-ΔuPAR clones (#3 and #6), was up to 2.5 times higher compared to the control (WT) and Neuro2a-uPAR cells (at 24 hr; Figure 4d). The treatment with uPA for 24 hr had no effect on

Neuro2a-ΔuPAR cell migration: No statistically significant difference was detected between Neuro2a-ΔuPAR cells cultured in control conditions (BSA) or upon uPA administration (at 24 hr; Figure 4d). The same results were demonstrated using highly specific uPA inhibitor BC11: administration of 10 μM BC11 did not affect significantly the migratory rate of Neuro2a cells ($p > .05$; two-way ANOVA). After 24 hr, we observed almost complete scratch closure in Neuro2a-ΔuPAR cell cultures (clones #3 and #6) (approximately, 75% in #3 clone and 87% in #6 clone, $p < .0001$; two-way ANOVA; Figure 4c). Taken together, the obtained results indicate that uPAR-deficient Neuro2a cells have a higher potential for migration in a wound scratch assay. Unexpectedly, uPA or BC11 administration to the culture media of cells with different uPAR expression exerted no stimulatory or inhibitory effect on cell migration, respectively.

3.7 | uPAR suppression upregulates expression of EMT proteins in Neuro2a cells

Since we obtained results on enhanced cell migration in uPAR-deficient neuroblastoma cells, we aimed to determine whether experimentally altered uPAR expression could influence the EMT program. To test this possibility, we first examined the expression of epithelial and mesenchymal markers in Neuro2a cells using western blot analysis (Figure 5). While we identified the substantial expression of epithelial markers, such as occludin, claudin-5, and E-cadherin in uPAR-expressing cells (WT and Neuro2a-uPAR cells; Figure 5a), the mesenchymal markers, such as N-cadherin and α-SMA were undetectable (Figure 5b). Interestingly, the expression of the same epithelial markers in uPAR-deficient cells (clones #3, #6, and #30) was dramatically decreased, while the expression of

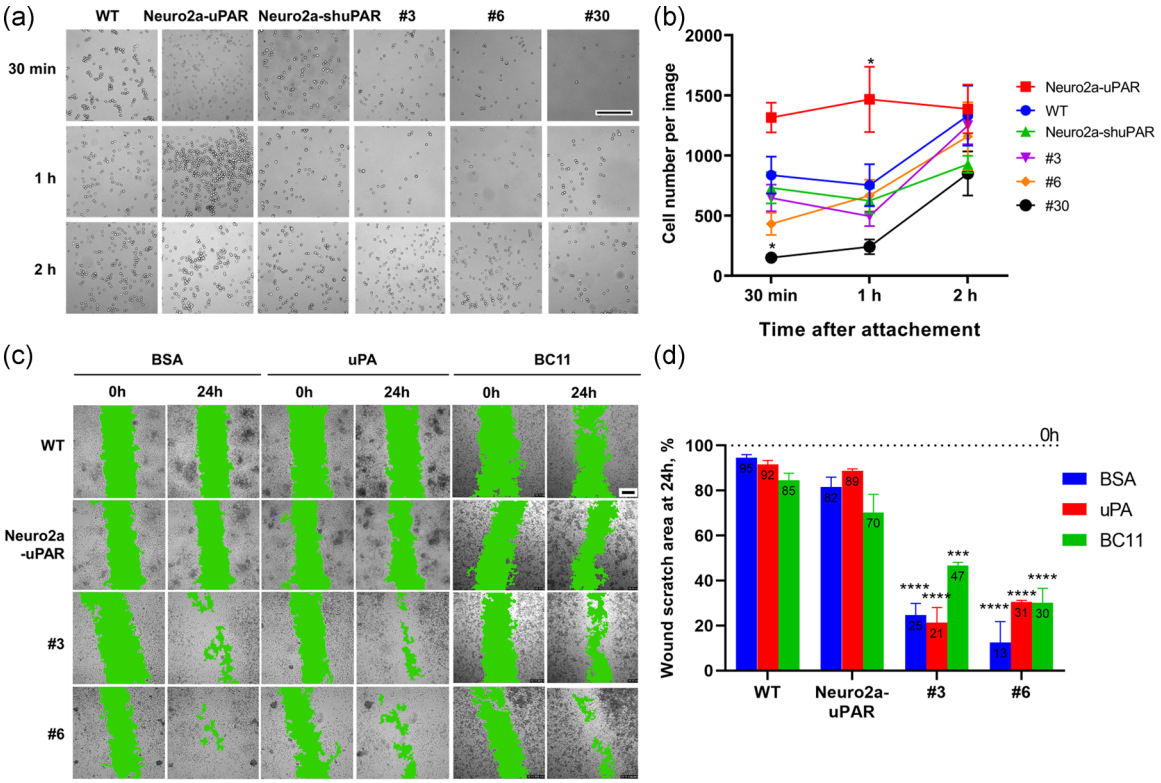

FIGURE 4 uPAR downregulation decreases Neuro2a cell adhesion and increases Neuro2a cell migration in wound scratch assay. (a) Neuro2a cells with different levels of uPAR expression were seeded into cell culture plates and the medium with non-adherent cells was replaced 30 min, 1 or 2 hr later. Neuro2a cell adhesion was analyzed using light microscopy. Bar 250 μm. Results are representative of three independent experiments. (b) Graph showing the mean number of attached cells calculated at least in three fields of view in three different wells ± *SEM*, *$p < .05$ compared with WT cells (two-way ANOVA, Tukey post hoc test). (c) Neuro2a cells were allowed to form a confluent monolayer. A scratch was created in a straight line with a p1000 pipet tip across the monolayer of cells. During 24 hr cells were cultured in the presence of 50 nM of uPA, 10 μM BC11 (uPA inhibitor) or BSA as a control. Green areas indicate cell-free zones as determined using the MRI Wound Healing Tool of ImageJ. Results are representative of three independent experiments. Bar 250 μm. (d) Statistical analysis of the wound scratch closure monitored over time in the presence of BSA (blue columns), uPA (red columns), or BC11 (green columns). Data are presented as the mean residual wound area at 24 hr as a percentage of the original wound area at 0 hr ± *SEM*. *$p < .05$, **$p < .01$, ***$p < .001$, ****$p < .0001$ all compared with the respective value in WT BSA, WT uPA, or WT BC11 (two-way ANOVA, Tukey post hoc test). The factor of different agents (BSA, uPA, or BC11) administrated to the cell medium was statistically nonsignificant ($p > .05$, two-way ANOVA). WT: control Neuro2a cells; Neuro2a-uPAR: uPAR-overexpressing Neuro2a cells; #3 and #6: uPAR-deficient clones of Neuro2a cells. ANOVA, analysis of variance; BSA, bovine serum albumin; MRI, magnetic resonance imaging; uPA, urokinase-type plasminogen activator; uPAR, urokinase-type plasminogen activator receptor; *SEM*, standard error of mean; WT, wild-type

mesenchymal markers was upregulated (Figure 5). These results and the data obtained in the wound scratch assay allow us to assume that uPAR is a factor that sustains the epithelial phenotype in neuroblastoma cells. uPAR downregulation promotes the transition of cells into a mesenchymal state, characterized by increased migration.

3.8 | Quantitative RT-PCR of Snai1 in Neuro2a cells

Quantitative RT-PCR was carried out to detect the relative expression level of transcription factor *Snai1* since it is referred to as EMT-inducing transcription factor directly binding and repressing E-cadherin promoter (Thiery, Acloque, Huang, & Nieto, 2009). The mRNA, encoding transcription factor *Snai1*, was significantly upregulated in uPAR-deficient clone #6 ($p < .001$; ANOVA), while in clone #3 there was a tendency for an increase in Snai1 mRNA ($p > .05$; ANOVA; Figure 5c). The level of mRNA in clone #30 was comparable to WT cells. Unexpectedly, the mRNA level of *Snai1* in uPAR-overexpressing cells was increased compared to WT cells, suggesting potentially complicated transcription machinery involved as a response to uPAR overexpression. We also compared the mRNA expression levels of *Slug*, *Zeb1*, *Zeb2*, and *Twist2* in cells with different uPAR expression, but no comprehensive results could be obtained (data not shown). Thus, although the data above clearly demonstrate the phenotype change from epithelial to mesenchymal in Neuro2a cells upon uPAR suppression (Figures 2 and 4), the lack of unequivocal data on the well-known EMT-transcription factor expression prompted us to search for other potential mechanisms involved in uPAR-related phenotype changes.

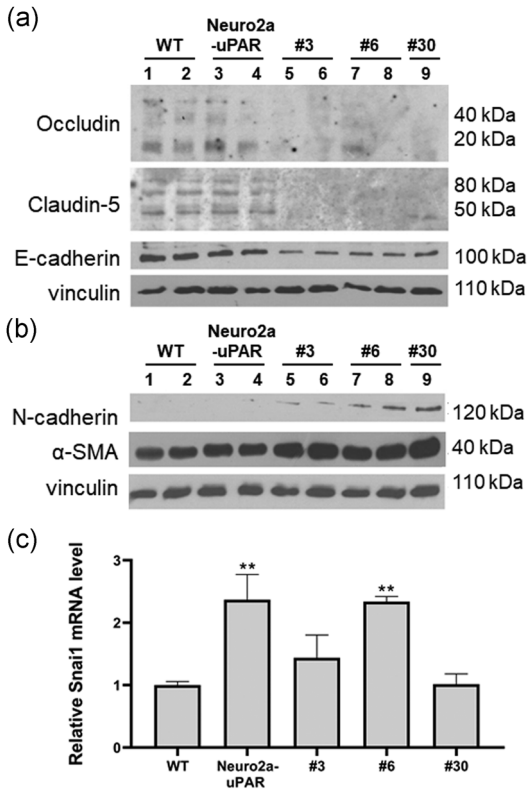

FIGURE 5 Expression of EMT markers in Neuro2a cells depends on the expression level of uPAR. Western blot analysis of epithelial (a) and mesenchymal (b) markers expression of EMT process was detected in Neuro2a cells. WT, Neuro2a-uPAR, #3 and #6 clones represented in the figure in duplicates. Vinculin was used as a protein loading control. Reproducible results of three independent experiments are presented. (c) The level of *Snail* expression depends on uPAR downregulation. The mRNA level of Snai1 was normalized to β-actin expression as a housekeeping gene; the normalization was done assuming the mean level of transcript in WT cells to be 1. The bar graph represents the mean relative expression level of at least three biological repeats ± *SEM*. $^{**}p < .01$ compared with WT cells (ANOVA, Tukey post hoc test). WT: control Neuro2a cells; Neuro2a-uPAR: uPAR-overexpressing Neuro2a cells; #3 and #6: uPAR-deficient clones of Neuro2a cells. α-SMA, α-smooth muscle actin; ANOVA, analysis of variance; EMT, epithelial–mesenchymal transition; mRNA, messenger RNA; *SEM*, standard error of mean; uPAR, urokinase-type plasminogen activator receptor; WT, wild-type

3.9 | uPAR suppression upregulates IL-6 expression in Neuro2a cells

It is well-known that the EMT in neuroblastoma, its invasiveness, and metastasis are orchestrated by several signaling pathways, including IL-6 and tumor growth factor-β/SMAD signaling (Ara et al., 2009; Kumari, Dwarakanath, Das, & Bhatt, 2016; Shao, Gao, Huang, & Lu, 2017; Tawara, Oxford, & Jorcyk, 2011). Western blot analysis substantiated the presence of IL-6 in the lysates of all tested cell types. uPAR overexpression resulted in reduced expression of IL-6 compared to WT cells (Figure 6a). However, in uPAR-deficient cells (clones #3, #6, and #30) we detected a significant increase in IL-6 content compared with WT and Neuro2a-uPAR cells. Thus, uPAR downregulation leads to increased IL-6 expression. Interestingly, we were not able to detect the activation of SMAD2 and SMAD3 by western blot analysis in Neuro2a cell lysates (p-SMAD2 and p-SMAD3 in Figure 6a), suggesting the involvement of other signal transduction mechanisms.

3.10 | uPAR-dependent nuclear translocation of p-ERK1/2 and STAT in Neuro2a cells

There is compelling evidence indicating the involvement of ERK1/2 in EMT in many cancers including neuroblastoma (Horn, Gaziel, Wreschner, Smorodinsky, & Ehrlich, 2009; Lim, Chuong, & Roy-Burman, 2011; Ma & Wells, 2014; Xie et al., 2004). In neuroblastoma cells, the binding of IL-6 to its receptor leads to the activation of signal transduction through Janus kinase (JAK), the STAT protein family, and ERK1/2 (Ara et al., 2009; Guo, Xu, Lu, Duan, & Zhang, 2012; Naveen, Gaikwad, & Agrawal-Rajput, 2016;

Tawara et al., 2011). Our results described above on the accumulation of IL-6 upon uPAR suppression and the lack of SMAD activation prompted us to hypothesize the involvement of ERK1/2 and STAT in the observed EMT in uPAR-deficient cells.

It is well-known that activated ERK1/2 can exert signaling effects on mitogen-activated protein kinase (MAPK) activity in the cytoplasm or can be directly translocated into the nucleus, where it regulates the activity of a number of transcription factors and genes responsible for EMT (Aguirre-Ghiso, Estrada, Liu, & Ossowski, 2003; Eden, Archinti, Furlan, Murphy, & Degryse, 2011; Nguyen et al., 1998).

To determine if uPAR can influence the activation state of ERK1/2, we analyzed the content of p-ERK1/2 (T185 and T202) in total lysates of Neuro2a cells with different levels of uPAR expression. Moreover, we fractionated cell lysates into the cytosolic and nuclear fractions to evaluate activated p-ERK1/2 in the subcellular compartments. As shown in Figure 6b,c, uPAR overexpression led to ERK1/2 activation and complete translocation of p-ERK1/2 into the nucleus, while in uPAR-deficient clones there was an insignificant reduction in p-ERK1/2 content detected in the cytosolic fraction compared to WT cells.

The consequences of STATs' activation result in their phosphorylation and translocation into the nucleus (Clevenger, 2004). To address the possible involvement of STAT in uPAR-mediated effects on EMT, we assessed the content of activated STAT1 that had been translocated to the nucleus in Neuro2a cells. As expected, STAT1 was increased in the nuclear fraction of uPAR-overexpressing cells, while in #3 and #6 clones the content was significantly diminished compared to WT cells; the reduction of STAT1 in clone #30 was quite moderate possible due to incomplete knockout of uPAR in this clone (Figure 6d,e). The obtained results suggest that uPAR expression can have a serious impact on signal transduction and

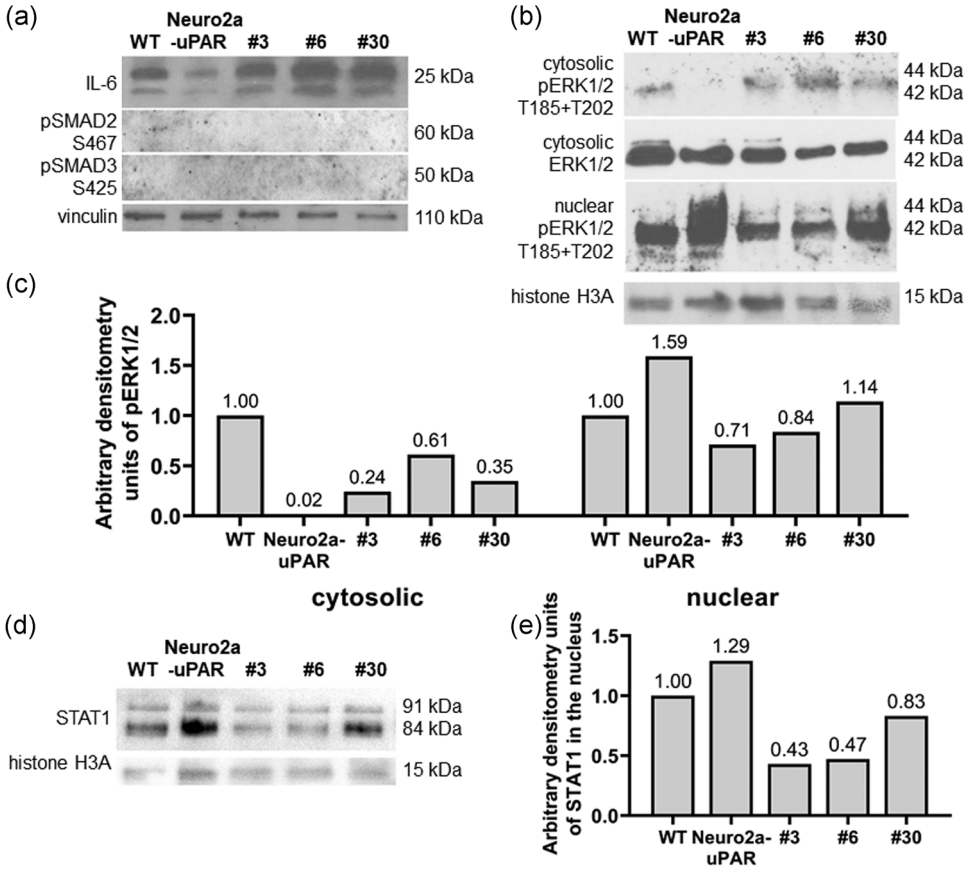

FIGURE 6 The effects of uPAR overexpression/suppression on IL-6 production, nuclear translocation of activated p-ERK1/2 and signal transducer and activator of transcription 1 (STAT1) in Neuro2a cells. (a) IL-6, p-SMAD2, and p-SMAD3 content were analyzed by western blot analysis in total cell lysates from Neuro2a cells with different levels of uPAR expression. Vinculin was used as a protein loading control. (b) Western blot analysis of the accumulation of p-ERK1/2 in the cytozolic and nuclear fractions from Neuro2a cells with different levels of uPAR expression. (c) Densitometry analysis of the cytozolic and nuclear p-ERK1/2 content. (d) The content of STAT1 in the nuclear fraction of Neuro2a cells was determined by western blot analysis. (e) Densitometry analyses of the STAT1 content in the nuclear fraction. In (b) and (d) Histone H3A was used as a protein loading control. WT: control Neuro2a cells; Neuro2a-uPAR: uPAR-overexpressing Neuro2a cells; #3, #6, and #30: uPAR-deficient Neuro2a clones. Results are representative of three independent experiments. IL-6, interleukin-6; p-ERK1/2, phospho-extracellular signal-regulated kinase 1/2; uPAR, urokinase-type plasminogen activator receptor; WT, wild-type

regulation of gene expression with the possible involvement of p-ERK1/2 and STAT1.

3.11 | uPAR-dependent nuclear accumulation of uPA and translocation of NF-κB into the nucleus of Neuro2a cells

Another well-known transcription regulator that promotes EMT and cancer is NF-κB (Chan et al., 2004; Kim et al., 2018; Park & Hong, 2016; Xia, Shen, & Verma, 2014). When NF-κB is activated, it is translocated from the cytoplasm into the nucleus where it regulates gene expression responsible for cell transformation, proliferation, apoptosis, invasion, and metastasis (Shishodia & Aggarwal, 2004). NF-κB can modulate IL-6/STAT signaling (Xia et al., 2014). Therefore, we aimed to determine whether NF-κB becomes activated and translocated to the nucleus in Neuro2a cells upon uPAR over-expression/suppression using WT, uPAR-overexpressing cells and uPA-deficient clones #3, #6, and #30. In addition, we enrolled Neuro2a clones #3, #6, and #30 which have been subjected to uPAR

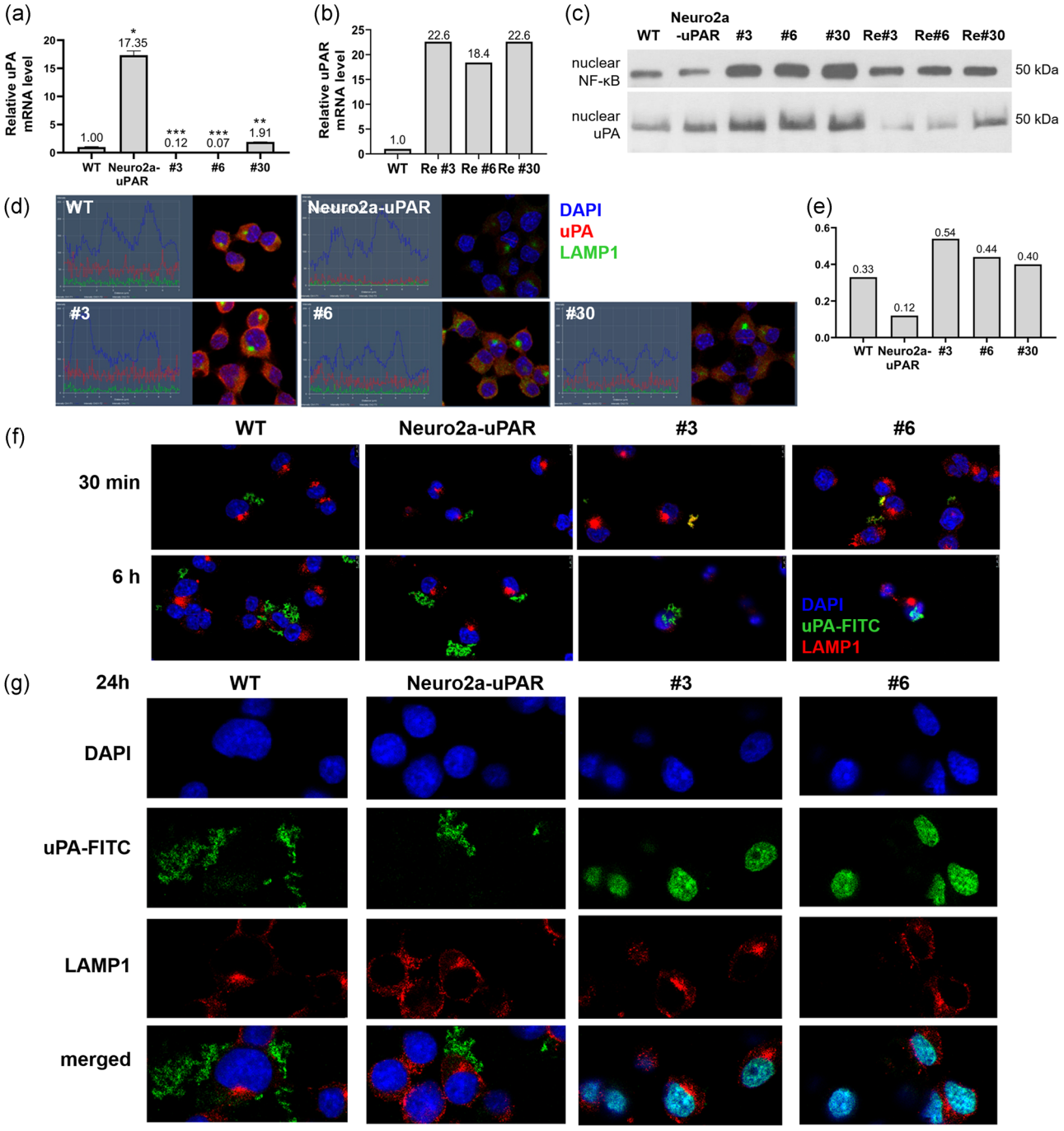

FIGURE 7 Continued.

re-expression using cDNA transient plasmid transfection. The relative uPAR mRNA expression was assessed using RT-PCR (Figure 7b). As shown in Figure 7c, NF-κB content in the nuclear fraction of uPAR-overexpressing cells was diminished compared with WT, while in all uPAR-deficient cells (clones #3, #6, and #30) NF-κB was significantly upregulated compared with WT. Moreover, uPAR re-expression in uPAR-deficient clones decreased NF-κB content in the nuclear fraction (Re#3, Re#6, and Re#30 clones) compared to the original clones. These data confirm the reliability of the obtained results on uPAR involvement in NF-κB activation and translocation to the nucleus as well as point to the possible involvement of uPAR in signal transduction and transcription regulation via NF-κB.

One of NF-κB downstream target genes is uPA (Chan et al., 2004). Recent studies suggest that uPA can exert pleiotropic effects on proliferation and migration in a uPAR-dependent manner (Blasi, 1999) or in a uPAR-independent manner via nucleolin-mediated translocation of uPA into the nucleus with the possible uPA-chromatin association that modulates transcriptional activity (Stepanova et al., 2008).

We first evaluated the uPA mRNA in Neuro2a cells with different uPAR expression. We observed a dramatic increase in uPA expression in Neuro2a-uPAR cells ($p < .05$; Welch's ANOVA) and a moderate increase in clone #30 ($p < .01$; Welch's ANOVA), while in clones #3 and #6 uPA expression was diminished compared to WT cells ($p < .001$, Welch's ANOVA; Figure 7a). We further tested the hypothesis that uPAR can affect uPA localization and function. Specifically, uPA in the absence of uPAR can be translocated to the nucleus and participate in the regulation of gene expression and EMT.

Western blot analysis demonstrated that uPA was present in the nuclear fraction of WT cells; uPAR overexpression (Neuro2a-uPAR) had no effect on the uPA level (Figure 7c). However, uPA content in the nuclear fraction in all Neuro2a-deficient clones (#3, #6, and #30) was significantly increased compared with WT. Moreover, after uPAR re-expression (clones Re#3, Re#6, and Re#30), uPA content was noticeably decreased to the level even lower than that of the original Neuro2a-ΔuPAR clones and was almost undetectable.

To confirm our western blot analysis results, we used confocal microscopy as described in Section 2. Double immunofluorescent staining using antibodies against uPA and LAMP1-lysosomal marker was carried out under permeabilizing conditions (Figure 7d). Nuclei were counterstained with DAPI. Figure 7d,e, show the subcellular distribution and immunofluorescence intensities. On the optical section passing through the region of the nucleus for each tested cell, a red arrow tool was used to denote the profile, quantified using the Histo function of ZEN 2010 software. For blue (DAPI), green (lysosome marker), and red (uPA) channels, we obtained the distribution of pixel intensities along the arrow. The presence of blue pixels further confirmed that the optical section was passing through the nucleus. The intensity of red fluorescence was correlated to the content of urokinase in the nucleus. The threshold was set using the intensity level in the green channel, since LAMP1 staining in the nucleus was considered to be nonspecific. Nuclear uPA-positive staining was evaluated in WT, Neuro2a-uPAR, and Neuro2a-ΔuPAR cells using equal imaging settings (Figure 7d). Surprisingly, uPAR expression affected the presence of uPA in the nucleus (Figure 7d,e). The intensity of uPA staining in control cells was 0.33 units, while uPAR overexpression resulted in the decrease in the intensity up to 0.12 units. On the contrary, in uPAR-deficient cells, the intensity of uPA staining significantly increased: For clone #3 up to 0.54, for clone #6 up to 0.44 and for clone #30 up to 0.40 units. In Neuro2a-uPAR cells, uPA co-localization with LAMP1 was markedly increased compared with WT cells, while in uPAR-deficient clones the co-localization signal was reduced (data not shown).

To address the question of the source of nuclear uPA, FITC-conjugated uPA was added to the wells with Neuro2a cells (Figure 7f). Immunofluorescent staining using antibodies against

FIGURE 7 Downregulation of uPAR in Neuro2a leads to uPA and NF-κB translocation into the nucleus. (a) RT-PCR analysis of *uPA* expression level. The mRNA level of uPA was normalized to β-actin expression as a housekeeping gene; the normalization was done assuming the mean level of transcript in WT cells to be 1. The bar graph represents the mean relative expression level of at least three biological repeats ± *SEM*. *$p < .05$, **$p < .01$, ***$p < .001$ compared with WT cells (unequal variances, Welch's ANOVA, Tamhane's T2 post hoc tests). (b) RT-PCR analysis was carried out to evaluate the expression of uPAR in control Neuro2a cells (WT) and clones after re-expression of uPAR (Re#3, Re#6, and Re#30). Data were normalized to β-actin expression as a housekeeping gene. Results are representative of three independent experiments. (c) Accumulation of uPA and NF-κB in the nuclear fractions of Neuro2a cells with different levels of uPAR expression using western blot analysis assay. Results are representative of three independent experiments. (d) Double immunofluorescent staining of Neuro2a cells with antibodies against uPA (red fluorescence) and LAMP1-lysosomal marker (green fluorescence). Nuclei were counterstained with DAPI (blue fluorescence). The results of at least three independent experiments are presented. The distribution of pixel intensity along the red arrow passing through the region of the nucleus is shown on the left side of each image. (e) Graph representing the results of the fluorescence intensity analysis of uPA content in the nuclei of Neuro2a cells. Results are representative of three independent experiments. (f) Confocal microscopy of Neuro2a cells 30 min and 6 hr after administration of FITC-conjugated uPA (green fluorescence) to the cell culture medium. Immunofluorescent staining using antibodies against LAMP1 (red fluorescence) was carried out under permeabilizing conditions, nuclei were counterstained with DAPI (blue fluorescence). The results of at least three independent experiments are presented. (g) The same experiment as in (f) after 24 hr incubation with uPA-FITC; channels are presented separately or merged (DAPI blue fluorescence, uPA-FITC green fluorescence, LAMP1 red fluorescence). The results of at least three independent experiments are presented. ANOVA, analysis of variance; DAPI, 4′,6-diamidino-2-phenylindole; FITC, fluorescein isothiocyanate; LAMP1, lysosomal-associated membrane protein; NF-κB, nuclear factor κB; mRNA, messenger RNA; RT-PCR, real-time polymerase chain reaction; *SEM*, standard error of mean; uPA, urokinase-type plasminogen activator; uPAR, urokinase-type plasminogen activator receptor; WT, wild-type

LAMP1 was carried out under permeabilizing conditions to visualize the proteins located in the cytoplasm using LAMP1 as a marker of lysosomes (Cheng et al., 2018). We used confocal microscopy to determine uPA-FITC localization after 30 min, 6 hr, and 24 hr of incubation. Thirty minutes after, exogenously administrated FITC-conjugated uPA was detected in the cytoplasm of uPAR-deficient clones #3 and #6 and colocalized with LAMP1 (yellow staining in Figure 7f). Six hours later (Figure 7f) and more strongly after 24 hr (Figure 7g), uPA-FITC fluorescence was mainly detected inside the nucleus in uPAR-deficient clones #3 and #6. In uPAR-expressing cells (Neuro2a-uPAR and WT) uPA-FITC was predominantly observed in the cytoplasm. Therefore, we infer that in the absence of uPAR on the cell surface extracellular uPA is rapidly transported into the nucleus.

Thus, our western blot analysis and confocal microscopy data suggest that uPAR functions as a uPA "trap" that forwards uPA for degradation in lysosomes, while in the absence of uPAR, extracellular uPA is translocated into the nucleus and is potentially involved in the regulation of gene expression.

4 | DISCUSSION

It is common knowledge that uPA and uPAR are present at the leading edge of migrating cells in vitro (Estreicher, Mühlhauser, Carpentier, Orci, & Vassalli, 1990; Jaiswal et al., 2018) and that the expression of uPA, PAI-1, and uPAR is increased during the migration of a number of different cells (Jaiswal et al., 2018). However, besides the enzymatic activity of uPA that facilitates cell migration via degradation of extracellular matrix (Blasi, 1999), uPA initiates downstream JAK/STAT, MAPK/ERK, and SMAD signaling cascades via uPA/uPAR interaction with integrins, vitronectin, and several transmembrane receptors (Eden et al., 2011; Nguyen et al., 1998). Interestingly, in some cell systems, the induction of intracellular signaling via uPAR is independent of uPA catalytic activity, as signaling can be induced by proteolytically inactive ATF (amino-terminal fragment of uPA) (Mekkawy et al., 2014). In our experimental settings, administration of an active recombinant uPA (ab92641; Abcam) or its specific inhibitor BC11 to the culture media exerted no effect on migration of Neuro2a cells with different levels of uPAR expression (Figure 4c,d), implicating that proteolytic activity is not important for cell migration and suggesting that transduction of migratory signals is rather involved.

uPAR was proved to interact with integrins directly and to regulate their conformation and function, cell adhesion, and migration (Mahmood, Mihalcioiu, & Rabbani, 2018). High level of uPAR expression and its interaction with integrins enhances the basal level of activated ERK and PI3K in different cancer cells and favors tumor growth in vitro and in vivo (Aguirre-Ghiso et al., 2003; Chandrasekar et al., 2003; Nguyen et al., 1998; Wei et al., 2007). Our observations recapitulate the results of the previous studies and demonstrate that uPAR overexpression results in STAT1 and ERK1/2 activation and their translocation into the nucleus in Neuro2a cells (Figure 6), where they presumably participate in the regulation of gene expression responsible for cell proliferation and/or EMT. We also show that uPAR expression is important for supporting the colony-forming potential of Neuro2a cells, since uPAR deficiency results in the diminished CFU reflecting either reduced proliferation or enhanced migration or both (Figures 2e,f and 4c,d).

Numerous data support the idea that EMT plays a central role in tumor growth and metastasis (Mekkawy et al., 2014; Thiery et al., 2009). EMT is a conserved cellular program that results in a change of cell shape, including the loss of cell-cell adhesion and cell polarity, and the acquisition of migratory and invasive properties (Thiery et al., 2009; Ye & Weinberg, 2015). The role of the uPA system in EMT in several cancers has been addressed before (Laurenzana et al., 2015; Lester, Jo, Montel, Takimoto, & Gonias, 2007; Randle, Clarke, Henderson, & Odero-Marah, 2013; Wang, Ma, & Zhang, 2017). Hypoxia-induced EMT in breast cancer MDA-MB-468 cells was accompanied by increased expression of uPAR and was blocked by uPAR gene-silencing in vitro (Lester et al., 2007). Silencing of endogenous uPA or inhibition of uPAR-activated cell signaling, involving Src, PI3K, or ERKs, resulted in the reversal of EMT in uPAR-overexpressing breast cancer MDA-MB-468 cells (Jo et al., 2009). The EMT profile of melanoma cells, characterized by enhanced invasiveness and increased uPAR expression in vitro and in vivo, was abrogated by application of uPAR antisense oligonucleotide (Laurenzana et al., 2015). It was shown that cancer cells undergoing EMT can acquire stem cell-like properties further promoting tumor growth and spreading (Jo et al., 2010; Mani et al., 2008; Thiery et al., 2009). Though in MCF-7 breast cancer cells uPAR overexpression failed to induce EMT, nevertheless, it still induced cancer stem cell-like properties along with an increase in tumor growth in SCID mice. Interestingly, in MCF-7 mammospheres, which display a well-defined epithelial acinus-like structure and E-cadherin expression on the plasma membrane, cell collapse into the central cavity was prevented by uPAR overexpression. The authors inferred that uPAR signaling may stabilize epithelial morphology (Acton, 2012, p. 1853). The discrepancy in these results could reflect the complexity of molecular mechanisms and signaling cross-talk activated by uPAR in different cellular systems. Data obtained in the present study indicate for the first time that uPAR is an important regulator of epithelial phenotype in neuroblastoma Neuro2a cells: uPAR suppression results in cell size enlargement and EMT, and is accompanied by decreased cell adhesion and increased migration (Figures 2 and 4a,b). Epithelial markers occludin, claudin-5, and E-cadherin are substantially expressed in control and uPAR-overexpressing cells, while uPAR suppression leads to a dramatic morphological change and an increase in the expression of mesenchymal markers (N-cadherin and α-SMA; Figure 5).

Several developmental transcription factors such as *Snai1*, *Twist*, *Slug*, and *Zeb* are known to regulate the EMT, inducing expression of mesenchymal markers (vimentin, α-SMA, N-cadherin) and repressing epithelial markers (E-cadherin, epithelial cytokeratins, claudin, and occludin; Jaiswal et al., 2018; Mani et al., 2008; Ye & Weinberg, 2015). These transcription factors can be expressed in different

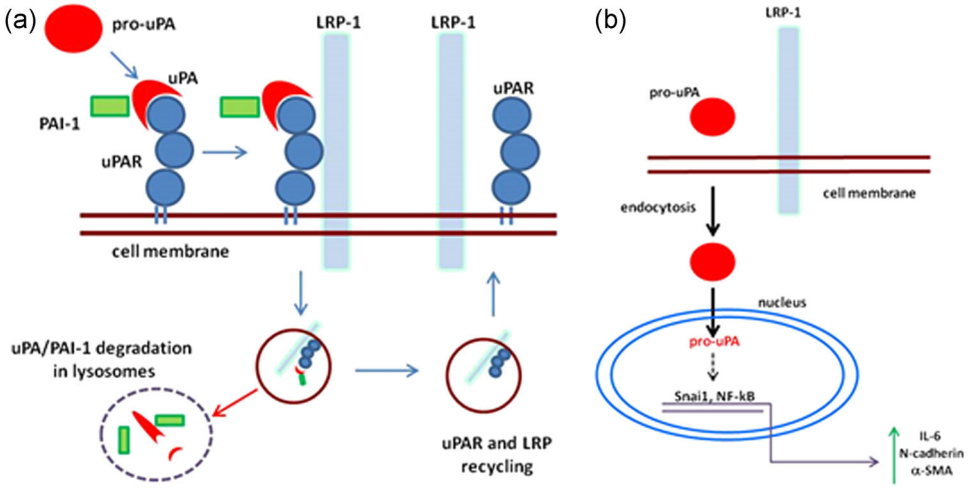

FIGURE 8 Final scheme of potential EMT regulation by uPA/uPAR cooperation in Neuro2a cells. (a) uPAR functions as a uPA "trap." When uPAR is expressed on the cell surface, binding of uPA to uPAR leads to rapid internalization of the ternary uPA/uPAR/PAI-1 complex via the LRP-1 receptor with subsequent lysosomal degradation of uPA and PAI-1; uPAR and LRP-1 recycle to the plasma membrane. (b) In the absence of uPAR, uPA is translocated to the nucleus, where it may be involved in the regulation of the activity of transcription factors Snai1 and NF-κB leading to increased expression of IL-6, N-cadherin, and α-SMA and resulting in epithelial to mesenchymal transition in Neuro2a cells. α-SMA, α-smooth muscle actin; EMT, epithelial–mesenchymal transition; IL-6, interleukin-6; LRP-1, LDL receptor-related protein 1; NF-κB, nuclear factor κB; uPA, urokinase-type plasminogen activator; uPAR, urokinase-type plasminogen activator receptor

combinations and can be upregulated in various types of malignancies (Hanahan & Weinberg, 2011). Here we have demonstrated that in uPAR-overexpressing Neuro2a cells mRNA level of *Snai1* (an important regulator of E-cadherin expression; Nieto, 2002) was substantially increased (Figure 5c). However, the results on *Slug*, *Zeb1*, *Zeb2*, and *Twist2* expression were ambiguous, underscoring the complexity of molecular interactions and suggesting the existence of other regulatory networks involving uPAR.

Another important regulator of EMT is NF-κB (Jaiswal et al., 2018; Thiery et al., 2009). NF-κB activity promotes tumor growth, suppresses apoptosis, and facilitates distant metastasis (Xia et al., 2014). NF-κB was shown to control uPA system expression by binding to cognate sequence elements of uPA promoter in different cancer cells (Baek et al., 2008; Chan et al., 2004; Sliva, 2004). We evaluated NF-κB expression and demonstrated that NF-κB content in the nuclear fraction was significantly increased in uPAR-deficient cells compared with the control, while in uPAR-overexpressing cells we found the opposite effect (Figure 7b). These results were further ratified by experiments on uPAR re-expression in uPAR-deficient clones, where NF-κB content was decreased compared to the original clones (Figure 7b), suggesting the existence of a regulatory loop between uPAR and NF-κB expression.

NF-κB activation also stimulates IL-6 production (Tawara et al., 2011). On the one hand, gp130 is a component of the IL-6 receptor complex, which is involved in regulation of cell proliferation, differentiation and migration (Guo et al., 2012; Scheller, Chalaris, Schmidt-Arras, & Rose-John, 2011; Weissenbach et al., 2004). On the other hand, gp130 is activated upon uPAR clustering and may serve as a transmembrane adapter activating JAK-STAT and ERK1/2 signaling pathways downstream of uPAR (Ara et al., 2009; Blasi & Carmeliet, 2002; Mahmood et al., 2018). Derangements in IL-6 signaling have been implicated in a large variety of cancers and metastasis (e.g., multiple myeloma, non-small cell lung carcinoma, colorectal cancer, renal cell carcinoma, prostate cancer, breast and ovarian cancers, neuroblastoma, etc; Guo et al., 2012; Tawara et al., 2011). Moreover, increased IL-6 production has been associated with neuroblastoma bone metastasis and poor prognosis (Tawara et al., 2011). IL-6/IL-6R/Stat3 signaling axis in breast cancer was shown to promote EMT, stemness, and cancer progression (Weng et al., 2019). Our data provide strong evidence that uPAR suppression results in the accumulation of IL-6 in Neuro2a cells, while uPAR overexpression exerts the opposite effect (Figure 6a). The exact mechanism is not clear and needs further clarification. However, the accumulation of IL-6 in uPAR-deficient clones correlates with EMT and enhanced cell migration, raising the possibility that an extensive cross-talk may occur linking uPAR-dependent and IL-6-activated signaling pathways in cancer.

Our recent data indicate that single-chain uPA upon binding to the cell surface and internalization can be rapidly translocated into the nucleus resulting in the direct interaction of uPA with nuclear transcription factors and gene expression regulation (Stepanova et al., 2008). We have demonstrated that for nuclear translocation uPA utilizes nucleolin, a nucleocytoplasmic shuttle (Stepanova et al., 2008). In human fibroblasts uPA nuclear translocation promotes upregulation of α-SMA expression in vitro (Stepanova et al., 2008) and in vivo uPA administration results in the transformation of vascular adventitial fibroblasts into myofibroblasts expressing α-SMA (Plekhanova et al., 2006). The results obtained in the present study favor a novel model: In the absence of uPAR in Neuro2a cells, extracellular uPA added to the conditioned media is translocated into the nucleus where it is involved in regulation of gene expression, EMT and the full spectrum of cellular changes (Figure 8), while in uPAR-expressing cells uPA activity and uPA/uPAR-mediated

signaling is tightly regulated by the lifespan of uPA/uPAR complex on the plasma membrane. Specifically, PAI-1 binds uPA/uPAR on the plasma membrane and the ternary uPAR/uPA/PAI-1 complex rapidly associates with LRP-1, resulting in its internalization and consequent uPA/PAI-1 degradation in the lysosomes, while uPAR and LRP-1 receptors recycle back to the cell surface (Conese et al., 1995; Czekay et al., 2001; Nykjaer et al., 1992).

The present study has certain limitations, since we used only one neuroblastoma cell line (Neuro2a). Therefore, the same mechanisms of uPAR functioning in other cancer cells need further investigation. The hypothesis on uPAR functioning as a uPA "trap," which takes into consideration the complexity of the molecular cascades and of the versatile signaling cross-talks activated by uPA system, provides a potential explanation for the delayed progress on targeting uPA and uPAR in clinics (see Video).

ACKNOWLEDGMENTS

This research was supported by the Russian Science Foundation (Project No. 19-75-30007) and Grant No. 17-04-00386 of the Russian Foundation of Basic Research. CRISPR/Cas9 *PLAUR* down-regulation, uPAR overexpression, and re-expression in Neuro2a cells were supported by Grant No. 17-04-00386, all other methods and research were supported by Project No. 19-75-30007.

CONFLICT OF INTERESTS

The authors declare that there are no conflict of interests.

AUTHORS CONTRIBUTIONS

E. V. S. and K. A. R. conceived and designed the experiments. E. V. S., A. A. S., K. D. R., P. S. K., N. A. A., V. Y. S., and M. N. K. performed the experiments, analyzed the data, and performed the statistical analyses. E. V. S. and K. A. R. contributed to the manuscript writing. V. A. T. made a substantial contribution to the conception of the manuscript. All authors read and approved the final manuscript.

DATA AVAILABILITY STATEMENT

Data are available on request from the corresponding author.

ORCID

Ekaterina V. Semina http://orcid.org/0000-0002-3927-9286
Kseniya A. Rubina http://orcid.org/0000-0002-7166-7406
Anna A. Shmakova http://orcid.org/0000-0001-7162-074X
Karina D. Rysenkova http://orcid.org/0000-0003-1325-4002
Polina S. Klimovich http://orcid.org/0000-0002-8260-5542
Natalya A. Aleksanrushkina http://orcid.org/0000-0003-4946-7843
Veronika Y. Sysoeva http://orcid.org/0000-0001-9885-9056
Maxim N. Karagyaur http://orcid.org/0000-0003-4289-3428
Vsevolod A. Tkachuk http://orcid.org/0000-0002-7492-747X

REFERENCES

Acton, Q. A. (Ed.), 2012). *Cancer: New insights for the healthcare professional* (2011 ed.). Atlanta, Georgia: Scolarly Editions TM.

Aguirre-Ghiso, J. A., Estrada, Y., Liu, D., & Ossowski, L. (2003). ERK(MAPK) activity as a determinant of tumor growth and dormancy; regulation by p38(SAPK). *Cancer Research*, *63*(7), 1684–1695.

Ara, T., Song, L., Shimada, H., Keshelava, N., Russell, H. V., Metelitsa, L. S., & DeClerck, Y. A. (2009). Interleukin-6 in the bone marrow microenvironment promotes the growth and survival of neuroblastoma cells. *Cancer Research*, *69*(1), 329–337. https://doi.org/10.1158/0008-5472.CAN-08-0613

Baek, M. K., Kim, M. H., Jang, H. J., Park, J. S., Chung, I. J., Shin, B. A., & Jung, Y. D. (2008). EGF stimulates uPAR expression and cell invasiveness through ERK, AP-1, and NF-kappaB signaling in human gastric carcinoma cells. *Oncology Reports*, *20*(6), 1569–1575.

Baviskar, S. N. (2011). A quick and automated method for measuring cell area using ImageJ. *The American Biology Teacher*, *73*(9), 554–556. https://doi.org/10.1525/abt.2011.73.9.9

Blasi, F. (1999). Proteolysis, cell adhesion, chemotaxis, and invasiveness are regulated by the u-PA-u-PAR-PAI-1 system. *Thrombosis and Haemostasis*, *82*(2), 298–304.

Blasi, F., & Carmeliet, P. (2002). uPAR: A versatile signalling orchestrator. *Nature Reviews Molecular Cell Biology*, *3*(12), 932–943. https://doi.org/10.1038/nrm977

Blasi, F., & Sidenius, N. (2010). The urokinase receptor: Focused cell surface proteolysis, cell adhesion and signaling. *FEBS Letters*, *584*(9), 1923–1930. https://doi.org/10.1016/j.febslet.2009.12.039

Carlin, R., Davis, D., Weiss, M., Schultz, B., & Troyer, D. (2006). Expression of early transcription factors Oct-4, Sox-2 and Nanog by porcine umbilical cord (PUC) matrix cells. *Reproductive Biology and Endocrinology*, *4*(1), 8. https://doi.org/10.1186/1477-7827-4-8

Chan, C. F., Yau, T. O., Jin, D. Y., Wong, C. M., Fan, S. T., & Ng, I. O. (2004). Evaluation of nuclear factor-kB, urokinase-type plasminogen activator, and HBx and their clinicopathological significance in hepatocellular carcinoma. *Clinical Cancer Research*, *10*(12), 4140–4149. https://doi.org/10.1158/1078-0432.CCR-03-0574

Chandrasekar, N., Mohanam, S., Gujrati, M., Olivero, W. C., Dinh, D. H., & Rao, J. S. (2003). Downregulation of uPA inhibits migration and PI3k/Akt signaling in glioblastoma cells. *Oncogene*, *22*(3), 392–400. https://doi.org/10.1038/sj.onc.1206164

Chapin, J. C., & Hajjar, K. A. (2015). Fibrinolysis and the control of blood coagulation. *Blood Reviews*, *29*(1), 17–24. https://doi.org/10.1016/j.blre.2014.09.003

Cheng, X. T., Xie, Y. X., Zhou, B., Huang, N., Farfel-Becker, T., & Sheng, Z. H. (2018). Characterization of LAMP1-labeled nondegradative lysosomal and endocytic compartments in neurons. *Journal of Cell Biology*, *217*(9), 3127–3139. https://doi.org/10.1083/jcb.201711083

Choong, P. F., & Nadesapillai, A. P. (2003). Urokinase plasminogen activator system: A multifunctional role in tumor progression and metastasis. *Clinical Orthopaedics and Related Research*, (415 Suppl), S46–S58. https://doi.org/10.1097/01.blo.0000093845.72468.bd

Clevenger, C. V. (2004). Roles and regulation of stat family transcription factors in human breast cancer. *The American Journal of Pathology*, *165*(5), 1449–1460. https://doi.org/10.1016/S0002-9440(10)63403-7

Conese, M., Nykjaer, A., Petersen, C. M., Cremona, O., Pardi, R., Andreasen, P. A., & Blasi, F. (1995). alpha-2 Macroglobulin receptor/Ldl receptor-related protein(Lrp)-dependent internalization of the urokinase receptor. *The Journal of Cell Biology*, *131*(6), 1609–1622.

Cortese, K., Sahores, M., Madsen, C. D., Tacchetti, C., & Blasi, F. (2008). Clathrin and LRP-1-independent constitutive endocytosis and recycling of uPAR. *PLoS One*, *3*(11), e3730. https://doi.org/10.1371/journal.pone.0003730

Czekay, R. P., Kuemmel, T. A., Orlando, R. A., & Farquhar, M. G. (2001). Direct binding of occupied urokinase receptor (uPAR) to LDL receptor-related protein is required for endocytosis of uPAR and regulation of cell surface urokinase activity. *Molecular Biology of the Cell*, *12*(5), 1467–1479. https://doi.org/10.1091/mbc.12.5.1467

Degryse, B. (2008). The urokinase receptor and integrins constitute a cell migration signalosome. *The Cancer Degradome*, 451–474. https://doi.org/10.1007/978-0-387-69057-5_23

Eden, G., Archinti, M., Furlan, F., Murphy, R., & Degryse, B. (2011). The urokinase receptor interactome. *Current Pharmaceutical Design*, *17*(19), 1874–1889. https://doi.org/10.2174/138161211796718215

Ellis, V., Scully, M. F., & Kakkar, V. V. (1989). Plasminogen activation initiated by single-chain urokinase-type plasminogen activator. Potentiation by U937 monocytes. *The Journal of Biological Chemistry*, *264*(4), 2185–2188.

Estreicher, A., Mühlhauser, J., Carpentier, J. L., Orci, L., & Vassalli, J. D. (1990). The receptor for urokinase type plasminogen activator polarizes expression of the protease to the leading edge of migrating monocytes and promotes degradation of enzyme inhibitor complexes. *The Journal of Cell Biology*, *111*(2), 783–792. https://doi.org/10.1083/jcb.111.2.783

Fleetwood, A. J., Achuthan, A., Schultz, H., Nansen, A., Almholt, K., Usher, P., & Hamilton, J. A. (2014). Urokinase plasminogen activator is a central regulator of macrophage three-dimensional invasion, matrix degradation, and adhesion. *The Journal of Immunology*, *192*(8), 3540–3547. https://doi.org/10.4049/jimmunol.1302864

Gagliardi, A., Mullin, N. P., Ying Tan, Z., Colby, D., Kousa, A. I., Halbritter, F., & Chambers, I. (2013). A direct physical interaction between Nanog and Sox2 regulates embryonic stem cell self-renewal. *The EMBO Journal*, *32*(16), 2231–2247. https://doi.org/10.1038/emboj.2013.161

Gondi, C. S., Lakka, S. S., Dinh, D. H., Olivero, W. C., Gujrati, M., & Rao, J. S. (2004). Downregulation of uPA, uPAR and MMP-9 using small, interfering, hairpin RNA (siRNA) inhibits glioma cell invasion, angiogenesis and tumor growth. *Neuron Glia Biology*, *1*(2), 165–176. https://doi.org/10.1017/s1740925x04000237

Guo, Y., Xu, F., Lu, T., Duan, Z., & Zhang, Z. (2012). Interleukin-6 signaling pathway in targeted therapy for cancer. *Cancer Treatment Reviews*, *38*(7), 904–910. https://doi.org/10.1016/j.ctrv.2012.04.007

Hanahan, D., & Weinberg, R. A. (2011). Hallmarks of cancer: The next generation. *Cell*, *144*(5), 646–674. https://doi.org/10.1016/j.cell.2011.02.013

Horn, G., Gaziel, A., Wreschner, D. H., Smorodinsky, N. I., & Ehrlich, M. (2009). ERK and PI3K regulate different aspects of the epithelial to mesenchymal transition of mammary tumor cells induced by truncated MUC1. *Experimental Cell Research*, *315*(8), 1490–1504. https://doi.org/10.1016/j.yexcr.2009.02.011

Jaiswal, R. K., Varshney, A. K., & Yadava, P. K. (2018). Diversity and functional evolution of the plasminogen activator system. *Biomedicine & Pharmacotherapy*, *98*, 886–898. https://doi.org/10.1016/j.biopha.2018.01.029

Jo, M., Eastman, B. M., Webb, D. L., Stoletov, K., Klemke, R., & Gonias, S. L. (2010). Cell signaling by urokinase-type plasminogen activator receptor induces stem cell-like properties in breast cancer cells. *Cancer Research*, *70*(21), 8948–8958. https://doi.org/10.1158/0008-5472.CAN-10-1936

Jo, M., Lester, R. D., Montel, V., Eastman, B., Takimoto, S., & Gonias, S. L. (2009). Reversibility of epithelial–mesenchymal transition (EMT) Induced in breast cancer cells by activation of urokinase receptor-dependent cell signaling. *Journal of Biological Chemistry*, *284*(34), 22825–22833. https://doi.org/10.1074/jbc.M109.023960

Kim, G. C., Kwon, H. K., Lee, C. G., Verma, R., Rudra, D., Kim, T., & Im, S. H. (2018). Upregulation of Ets1 expression by NFATc2 and NFKB1/RELA promotes breast cancer cell invasiveness. *Oncogenesis*, *7*(11), 91. https://doi.org/10.1038/s41389-018-0101-3

Kumari, N., Dwarakanath, B. S., Das, A., & Bhatt, A. N. (2016). Role of interleukin-6 in cancer progression and therapeutic resistance. *Tumor Biology*, *37*(9), 11553–11572. https://doi.org/10.1007/s13277-016-5098-7

Kurtzberg, L. S., Battle, T., Rouleau, C., Bagley, R. G., Agata, N., Yao, M., & Teicher, B. A. (2008). Bone marrow and tumor cell colony-forming units and human tumor xenograft efficacy of noncamptothecin and camptothecin topoisomerase I inhibitors. *Molecular Cancer Therapeutics*, *7*(10), 3212–3222. https://doi.org/10.1158/1535-7163.MCT-08-0568

Laurenzana, A., Biagioni, A., Bianchini, F., Peppicelli, S., Chillà, A., Margheri, F., & Fibbi, G. (2015). Inhibition of uPAR-TGFβ crosstalk blocks MSC-dependent EMT in melanoma cells. *Journal of Molecular Medicine*, *93*(7), 783–794. https://doi.org/10.1007/s00109-015-1266-2

Lester, R. D., Jo, M., Montel, V., Takimoto, S., & Gonias, S. L. (2007). uPAR induces epithelial–mesenchymal transition in hypoxic breast cancer cells. *The Journal of Cell Biology*, *178*(3), 425–436. https://doi.org/10.1083/jcb.200701092

Li, X. Y., Zhou, X., Rowe, R. G., Hu, Y., Schlaepfer, D. D., Ilić, D., & Weiss, S. J. (2011). Snail1 controls epithelial–mesenchymal lineage commitment in focal adhesion kinase-null embryonic cells. *The Journal of Cell Biology*, *195*(5), 729–738. https://doi.org/10.1083/jcb.201105103

Liang, C. C., Park, A. Y., & Guan, J. L. (2007). In vitro scratch assay: A convenient and inexpensive method for analysis of cell migration in vitro. *Nature Protocols*, *2*(2), 329–333. https://doi.org/10.1038/nprot.2007.30

Lim, M., Chuong, C. M., & Roy-Burman, P. (2011). PI3K, ERK signaling in BMP7-Induced epithelial–mesenchymal transition (EMT) of PC-3 prostate cancer cells in 2- and 3-dimensional cultures. *Hormones and Cancer*, *2*(5), 298–309. https://doi.org/10.1007/s12672-011-0084-4

Luo, J., Sun, X., Gao, F., Zhao, X., Zhong, B., Wang, H., & Sun, Z. (2011). Effects of ulinastatin and docetaxel on breast cancer invasion and expression of uPA, uPAR, and ERK. *Journal of Experimental & Clinical Cancer Research*, *30*(1), 71. https://doi.org/10.1186/1756-9966-30-71

Ma, B., & Wells, A. (2014). The mitogen-activated protein (MAP) kinases p38 and extracellular signal-regulated kinase (ERK) are involved in hepatocyte-mediated phenotypic switching in prostate cancer cells. *Journal of Biological Chemistry*, *289*(16), 11153–11161. https://doi.org/10.1074/jbc.M113.540237

Mahmood, N., Mihalcioiu, C., & Rabbani, S. A. (2018). Multifaceted role of the urokinase-type plasminogen activator (uPA) and its receptor (uPAR): Diagnostic, prognostic, and therapeutic applications. *Frontiers in Oncology*, *8*, 24. https://doi.org/10.3389/fonc.2018.00024

Manetti, M., Rosa, I., Milia, A. F., Guiducci, S., Carmeliet, P., Ibba-Manneschi, L., & Matucci-Cerinic, M. (2014). Inactivation of urokinase-type plasminogen activator receptor (uPAR) gene induces dermal and pulmonary fibrosis and peripheral microvasculopathy in mice: A new model of experimental scleroderma? *Annals of the Rheumatic Diseases*, *73*(9), 1700–1709. https://doi.org/10.1136/annrheumdis-2013-203706

Mani, S. A., Guo, W., Liao, M. -J., Eaton, E. N., Ayyanan, A., Zhou, A. Y., & Weinberg, R. A. (2008). The epithelial–mesenchymal transition generates cells with properties of stem cells. *Cell*, *133*(4), 704–715. https://doi.org/10.1016/j.cell.2008.03.027

Mekkawy, A. H., Pourgholami, M. H., & Morris, D. L. (2014). Involvement of urokinase-type plasminogen activator system in cancer: An overview. *Medicinal Research Reviews*, *34*(5), 918–956. https://doi.org/10.1002/med.21308

Montuori, N., Pesapane, A., Rossi, F. W., Giudice, V., De Paulis, A., Selleri, C., & Ragno, P. (2016). Urokinase type plasminogen activator receptor

(uPAR) as a new therapeutic target in cancer. *Translational Medicine at UniSa*, *15*, 15–21.

Montuori, N., & Ragno, P. (2009). Multiple activities of a multifaceted receptor: Roles of cleaved and soluble uPAR. *Frontiers in Bioscience (Landmark Edition)*, *14*, 2494–2503.

Naveen, C. R., Gaikwad, S., & Agrawal-Rajput, R. (2016). Berberine induces neuronal differentiation through inhibition of cancer stemness and epithelial–mesenchymal transition in neuroblastoma cells. *Phytomedicine*, *23*(7), 736–744. https://doi.org/10.1016/J.PHYMED.2016.03.013

Nguyen, D. H., Hussaini, I. M., & Gonias, S. L. (1998). Binding of urokinase-type plasminogen activator to its receptor in MCF-7 cells activates extracellular signal-regulated kinase 1 and 2 which is required for increased cellular motility. *The Journal of Biological Chemistry*, *273*(14), 8502–8507.

Nieto, M. A. (2002). The snail superfamily of zinc-finger transcription factors. *Nature Reviews Molecular Cell Biology*, *3*(3), 155–166. https://doi.org/10.1038/nrm757

Nykjaer, A., Petersen, C. M., Møller, B., Jensen, P. H., Moestrup, S. K., Holtet, T. L., & Andreasen, P. A. (1992). Purified alpha 2-macroglobulin receptor/LDL receptor-related protein binds urokinase.plasminogen activator inhibitor type-1 complex. Evidence that the alpha 2-macroglobulin receptor mediates cellular degradation of urokinase receptor-bound complexes. *The Journal of Biological Chemistry*, *267*(21), 14543–14546.

Osorno, R., & Chambers, I. (2011). Transcription factor heterogeneity and epiblast pluripotency. *Philosophical Transactions of the Royal Society, B: Biological Sciences*, *366*(1575), 2230–2237. https://doi.org/10.1098/rstb.2011.0043

Park, M., & Hong, J. (2016). Roles of NF-κB in cancer and inflammatory diseases and their therapeutic approaches. *Cells*, *5*(2), 15. https://doi.org/10.3390/cells5020015

Plekhanova, O. S., Stepanova, V. V., Ratner, E. I., Bobik, A., Tkachuk, V. A., & Parfyonova, Y. V. (2006). Urokinase plasminogen activator in injured adventitia increases the number of myofibroblasts and augments early proliferation. *Journal of Vascular Research*, *43*(5), 437–446. https://doi.org/10.1159/000094906

Rabbani, S. A., Ateeq, B., Arakelian, A., Valentino, M. L., Shaw, D. E., Dauffenbach, L. M., & Mazar, A. P. (2010). An anti-urokinase plasminogen activator receptor antibody (ATN-658) blocks prostate cancer invasion, migration, growth, and experimental skeletal metastasis in vitro and in vivo. *Neoplasia*, *12*(10), 778–788. https://doi.org/10.1593/neo.10296

Randle, D. D., Clarke, S., Henderson, V., & Odero-Marah, V. A. (2013). Snail mediates invasion through uPA/uPAR and the MAPK signaling pathway in prostate cancer cells. *Oncology Letters*, *6*(6), 1767–1773. https://doi.org/10.3892/ol.2013.1635

Rysenkova, K. D., Semina, E. V., Karagyaur, M. N., Shmakova, A. A., Dyikanov, D. T., Vasiluev, P. A., & Tkachuk, V. A. (2018). CRISPR/Cas9 nickase mediated targeting of urokinase receptor gene inhibits neuroblastoma cell proliferation. *Oncotarget*, *9*(50), 29414–29430. https://doi.org/10.18632/oncotarget.25647

Santibanez, J. F. (2013). Transforming growth factor-beta and urokinase-type plasminogen activator: Dangerous partners in tumorigenesis—Implications in skin cancer. *ISRN Dermatology*, *2013*, 597927–26. https://doi.org/10.1155/2013/597927

Scheller, J., Chalaris, A., Schmidt-Arras, D., & Rose-John, S. (2011). The pro- and anti-inflammatory properties of the cytokine interleukin-6. *Biochimica et Biophysica Acta (BBA): Molecular Cell Research*, *1813*(5), 878–888. https://doi.org/10.1016/j.bbamcr.2011.01.034

Semina, E., Rubina, K., Sysoeva, V., Rysenkova, K., Klimovich, P., Plekhanova, O., & Tkachuk, V. (2016). Urokinase and urokinase receptor participate in regulation of neuronal migration, axon growth, and branching. *European Journal of Cell Biology*, *95*(9), 295–310. https://doi.org/10.1016/j.ejcb.2016.05.003

Shao, J. B., Gao, Z. M., Huang, W. Y., & Lu, Z. B. (2017). The mechanism of epithelial–mesenchymal transition induced by TGF-β1 in neuroblastoma cells. *International Journal of Oncology*, *50*(5), 1623–1633. https://doi.org/10.3892/ijo.2017.3954

Shishodia, S., & Aggarwal, B. B. (2004). Nuclear factor-κB: A friend or a foe in cancer? *Biochemical Pharmacology*, *68*(6), 1071–1080. https://doi.org/10.1016/j.bcp.2004.04.026

Sliva, D. (2004). Signaling pathways responsible for cancer cell invasion as targets for cancer therapy. *Current Cancer Drug Targets*, *4*(4), 327–336.

Solberg, H., Ploug, M., Høyer–Hansen, G., Nielsen, B. S., & Lund, L. R. (2001). The murine receptor for urokinase-type plasminogen activator is primarily expressed in tissues actively undergoing remodeling. *Journal of Histochemistry & Cytochemistry*, *49*(2), 237–246. https://doi.org/10.1177/002215540104900211

Stepanova, V., Lebedeva, T., Kuo, A., Yarovoi, S., Tkachuk, S., Zaitsev, S., & Cines, D. B. (2008). Nuclear translocation of urokinase-type plasminogen activator. *Blood*, *112*(1), 100–110. https://doi.org/10.1182/blood-2007-07-104455

Sugiura, Y., Ma, L., Sun, B., Shimada, H., Laug, W. E., Seeger, R. C., & DeClerck, Y. A. (1999). The plasminogen-plasminogen activator (PA) system in neuroblastoma: Role of PA inhibitor-1 in metastasis. *Cancer Research*, *59*(6), 1327–1336.

Tawara, K., Oxford, J. T., & Jorcyk, C. L. (2011). Clinical significance of interleukin (IL)-6 in cancer metastasis to bone: Potential of anti-IL-6 therapies. *Cancer Management and Research*, *3*, 177–189. https://doi.org/10.2147/CMR.S18101

Teesalu, T., Blasi, F., & Talarico, D. (1996). Embryo implantation in mouse: Fetomaternal coordination in the pattern of expression of uPA, uPAR, PAI-1, and alpha 2MR/LRP genes. *Mechanisms of Development*, *56*(1–2), 103–116.

Thiery, J. P., Acloque, H., Huang, R. Y. J., & Nieto, M. A. (2009). Epithelial–mesenchymal transitions in development and disease. *Cell*, *139*(5), 871–890. https://doi.org/10.1016/j.cell.2009.11.007

Ulisse, S., Baldini, E., Sorrenti, S., & D'Armiento, M. (2009). The urokinase plasminogen activator system: A target for anti-cancer therapy. *Current Cancer Drug Targets*, *9*(1), 32–71.

Walker, E., & Stanford, W. L. (2009). Transcriptional networks regulating embryonic stem cell fate decisions. *Regulatory Networks in Stem Cells*, 87–100. https://doi.org/10.1007/978-1-60327-227-8_8

Wang, P., Ma, M., & Zhang, S. (2017). EGF-induced urokinase plasminogen activator receptor promotes epithelial to mesenchymal transition in human gastric cancer cells. *Oncology Reports*, *38*(4), 2325–2334. https://doi.org/10.3892/or.2017.5920

Wei, Y., Tang, C.-H., Kim, Y., Robillard, L., Zhang, F., Kugler, M. C., & Chapman, H. A. (2007). Urokinase receptors are required for 5 beta 1 Integrin-mediated signaling in tumor cells. *Journal of Biological Chemistry*, *282*(6), 3929–3939. https://doi.org/10.1074/jbc.M607989200

Weissenbach, M., Clahsen, T., Weber, C., Spitzer, D., Wirth, D., Vestweber, D., & Schaper, F. (2004). Interleukin-6 is a direct mediator of T cell migration. *European Journal of Immunology*, *34*(10), 2895–2906. https://doi.org/10.1002/eji.200425237

Weng, Y.-S., Tseng, H.-Y., Chen, Y.-A., Shen, P.-C., Al Haq, A. T., Chen, L.-M., & Hsu, H. -L. (2019). MCT-1/miR-34a/IL-6/IL-6R signaling axis promotes EMT progression, cancer stemness and M2 macrophage polarization in triple-negative breast cancer. *Molecular Cancer*, *18*(1), 42. https://doi.org/10.1186/s12943-019-0988-0

Xia, Y., Shen, S., & Verma, I. M. (2014). NF-kB, an active player in human cancers. *Cancer Immunology Research*, *2*(9), 823–830. https://doi.org/10.1158/2326-6066.CIR-14-0112

Xie, L., Law, B. K., Chytil, A. M., Brown, K. A., Aakre, M. E., & Moses, H. L. (2004). Activation of the Erk pathway is required for TGF-β1-induced EMT in vitro. *Neoplasia*, *6*(5), 603–610. https://doi.org/10.1593/neo.04241

Ye, X., & Weinberg, R. A. (2015). Epithelial–mesenchymal plasticity: A central regulator of cancer progression. *Trends in Cell Biology*, *25*(11), 675–686. https://doi.org/10.1016/j.tcb.2015.07.012

SUPPORTING INFORMATION

Additional supporting information may be found online in the Supporting Information section.

How to cite this article: Semina EV, Rubina KA, Shmakova AA, et al. Downregulation of uPAR promotes urokinase translocation into the nucleus and epithelial to mesenchymal transition in neuroblastoma. *J Cell Physiol*. 2020;235:6268–6286. https://doi.org/10.1002/jcp.29555